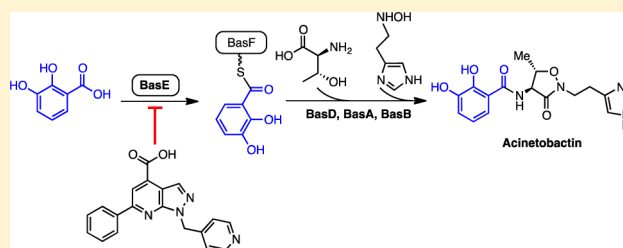


Non-Nucleoside Inhibitors of BasE, an Adenylating Enzyme in the Siderophore Biosynthetic Pathway of the Opportunistic Pathogen *Acinetobacter baumannii*João Neres,<sup>†,‡</sup> Curtis A. Engelhart,<sup>†,‡</sup> Eric J. Drake,<sup>§</sup> Daniel J. Wilson,<sup>†</sup> Peng Fu,<sup>†</sup> Helena I. Boshoff,<sup>||</sup> Clifton E. Barry, 3rd,<sup>||</sup> Andrew M. Gulick,<sup>§</sup> and Courtney C. Aldrich<sup>\*,†</sup><sup>†</sup>Center for Drug Design, Academic Health Center, University of Minnesota, Minneapolis, Minnesota 55455, United States<sup>‡</sup>Department of Medicinal Chemistry, University of Minnesota, Minneapolis, Minnesota 55455, United States<sup>§</sup>Hauptman-Woodward Institute and Department of Structural Biology, University at Buffalo, Buffalo, New York 14203-1102, United States<sup>||</sup>Tuberculosis Research Section, National Institute of Allergy and Infectious Diseases, Bethesda, Maryland 20892, United States

## S Supporting Information

**ABSTRACT:** Siderophores are small-molecule iron chelators produced by bacteria and other microorganisms for survival under iron limiting conditions such as found in a mammalian host. Siderophore biosynthesis is essential for the virulence of many important Gram-negative pathogens including *Acinetobacter baumannii*, *Klebsiella pneumoniae*, *Pseudomonas aeruginosa*, and *Escherichia coli*. We performed high-throughput screening against BasE, which is involved in siderophore biosynthesis in *A. baumannii*, and identified 6-phenyl-1-(pyridin-4-ylmethyl)-1H-pyrazolo[3,4-*b*]pyridine-4-carboxylic acid **15**. Herein we report the synthesis, biochemical, and microbiological evaluation of a systematic series of analogues of the HTS hit **15**. Analogue **67** is the most potent analogue with a  $K_D$  of 2 nM against BasE. Structural characterization of the inhibitors with BasE reveals that they bind in a unique orientation in the active site, occupying all three substrate binding sites, and thus can be considered as multisubstrate inhibitors. These results provide a foundation for future studies aimed at increasing both enzyme potency and antibacterial activity.



## ■ INTRODUCTION

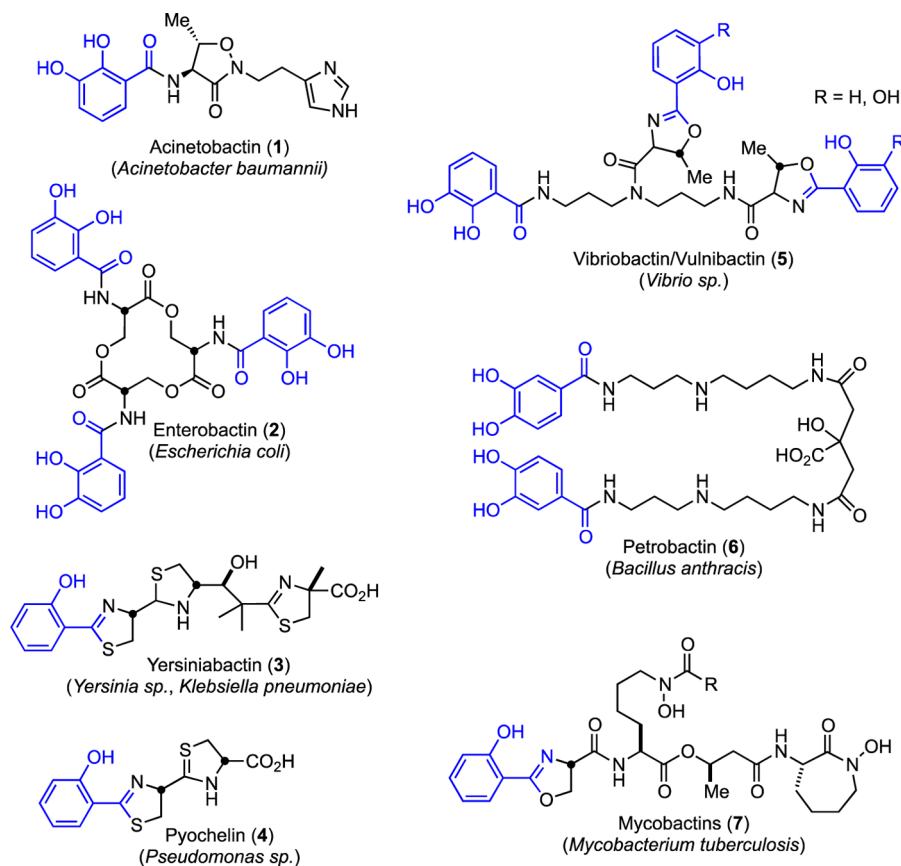
The increase of antibacterial resistance coupled with the lack of new antibiotics is cause for great concern.<sup>1,2</sup> This is highlighted by the Gram-negative bacteria *Acinetobacter baumannii*, an opportunistic organism that has emerged over the past couple of decades as one of the most insidious pathogens.<sup>3</sup> *A. baumannii* now accounts for more than 10% of hospital-acquired infections and is the leading cause of wound infections in soldiers in Iraq and Afghanistan.<sup>4,5</sup> Additionally, up to 30% of *A. baumannii* isolates in intensive care units are resistant to almost all known antibiotics including the  $\beta$ -lactams, fluoroquinolones, aminoglycosides, and tetracyclines.<sup>5</sup> According to the MYSTIC susceptibility data from 15 North American medical centers, *Acinetobacter* sensitivity is now below 60% for ceftazidime, cefepime, piperacillin/tazobactam, meropenem, imipenem, aztreonam, and gentamicin.<sup>6</sup> Comparative genomic studies of *A. baumannii* identified an unprecedented 86 kb cluster of 45 resistance genes in one particular strain.<sup>7,8</sup> The prevalence of the multidrug resistance (MDR) phenotype among Gram-negative pathogens including *A. baumannii* has led infectious disease physicians to reintroduce the colistins and polymyxins.<sup>9</sup> These related cationic lipopeptides were first introduced in the 1950s, but their use had been largely curtailed

by the 1980s as a result of their considerable nephrotoxicity.<sup>10</sup> *A. baumannii* clinical isolates have been reported that are no longer susceptible to these antibiotics of last resort.<sup>10</sup> It is astonishing to think that we may soon enter an era when antibiotic therapy is unavailable for previously treatable infections.

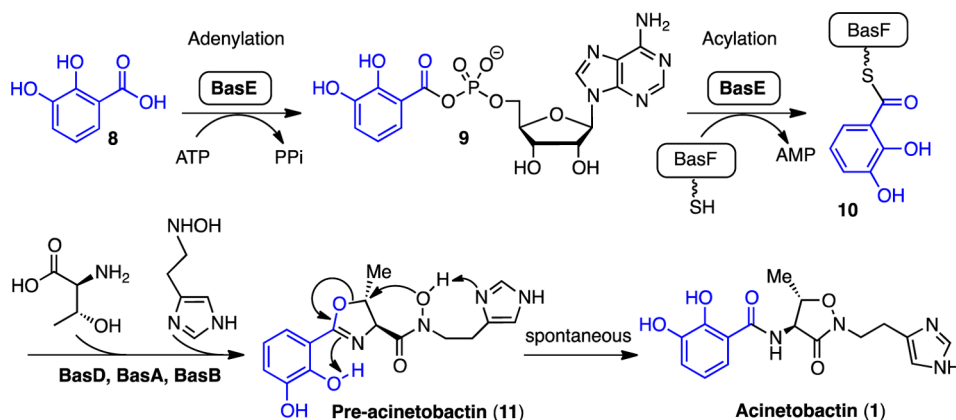
All bacteria with the exception of *Borrelia burgdorferi*<sup>11</sup> require micromolar levels of iron ( $\text{Fe}^{2+}/\text{Fe}^{3+}$ ) for growth, since iron serves as a cofactor in numerous biochemical processes.<sup>12</sup> However, the concentration of iron in serum and human body fluids is approximately  $10^{-24}$  M. The extraordinarily low concentration of free iron provides innate immunity to bacterial infections and is a result of the insolubility of iron(III) under aerobic conditions and the sequestration of the remaining free iron by the iron-binding proteins such as transferrin and lactoferrin. Many pathogens like *A. baumannii* overcome this iron limitation via the synthesis of siderophores, which are small-molecule high-affinity iron chelators secreted by bacteria and reimported from the external milieu after successfully chelating non-heme host iron (Figure 1).<sup>12–15</sup> The critical role

Received: November 20, 2012

Published: February 26, 2013



**Figure 1.** Structures of representative aryl-capped siderophores.



**Figure 2.** Biosynthesis of acinetobactin. BasE binds 2,3-dihydroxybenzoic acid **8** and ATP and then catalyzes their condensation to form an intermediate acyl-adenylate **9** that remains tightly bound. In the second half reaction, BasE catalyzes the transfer of the acyl group (blue) onto a nucleophilic sulfur atom of the aryl carrier domain of BasF to provide the acylated complex **10** with the release of AMP. Further steps are catalyzed by BasD, BasA, and BasB, incorporating threonine and *N*-hydroxyhistamine to yield pre-acinetobactin **11**. This molecule undergoes a facile rearrangement to the isoxazolidinone isomer of acinetobactin **1** that is likely promoted via an internal hydrogen bond with the oxazoline nitrogen atom in conjunction with the proximal imidazole moiety that serves to deprotonate the *N*-hydroxyamide functional group.

that siderophores play in virulence has been demonstrated in *A. baumannii*,<sup>16</sup> as well as in numerous other significant Gram-negative pathogens including *Klebsiella pneumoniae*,<sup>17</sup> *Pseudomonas aeruginosa*,<sup>18</sup> and *Escherichia coli*.<sup>19</sup> Siderophores are also critical for the virulence of many Gram-positive bacteria including *Bacillus anthracis*,<sup>20</sup> *Staphylococcus aureus*,<sup>21</sup> and the acid fast *Mycobacterium tuberculosis*.<sup>22</sup> Consequently, inhibition of siderophore biosynthesis represents a promising new strategy for antibacterial drug development, an approach that is further bolstered by the observation that many bactericidal antibiotics

ultimately operate through disruption of bacterial iron homeostasis and generation of reactive oxygen species (ROS).<sup>23,24</sup>

*A. baumannii* produces acinetobactin, a mixed ligand siderophore containing a catechol and imidazole for iron coordination.<sup>25,26</sup> The biosynthesis of acinetobactin is initiated by BasE that activates and loads 2,3-dihydroxybenzoic acid (DHB) onto a nonribosomal peptide synthetase (NRPS) pathway comprising four other proteins (BasF, BasD, BasA, and BasB).<sup>27,28</sup> This assembly line of proteins condenses DHB, L-

threonine, and *N*-hydroxyhistamine to afford pre-acinetobactin **11**, which spontaneously rearranges to acinetobactin **1** (Figure 2).<sup>29,30</sup> BasE represents an ideal target, since it does not possess a mammalian homologue, the protein has been biochemically and structurally characterized,<sup>31</sup> and the functionally related aminoacyl t-RNA synthetases are validated antibiotic targets with mupirocin the first in class inhibitor.<sup>32</sup> Homologues from other organisms as shown in Table 1 suggest that inhibitors may also be useful to combat several significant bacterial pathogens.

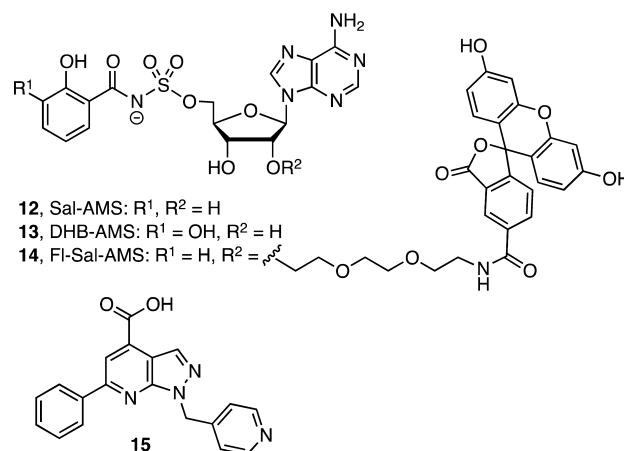
**Table 1. Aryl-Capped Siderophores Producing Pathogens and Corresponding AAAEs**

organism	siderophore	AAAE	AAAE substrate <sup>a</sup>
Gram-Negative			
<i>A. baumannii</i>	acinetobactin	BasE	DHB
<i>E. coli</i>	enterobactin	EntE	DHB
<i>K. pneumoniae</i>	yersiniabactin	YbtE	DHB
	enterobactin	EntE	SAL
<i>P. aeruginosa</i>	pyochelin	PchD	DHB
<i>Y. pestis</i>	yersiniabactin	YbtE	SAL
<i>Y. pseudotuberculosis</i>	yersiniabactin	YbtE	SAL
<i>V. cholerae</i>	vibriobactin	VibE	DHB
<i>V. vulnificus</i>	vulnibactin	VibE1	DHB
		VibE2	SAL
Gram-Positive			
<i>B. subtilis</i>	bacillibactin	DhbE	DHB
<i>B. anthracis</i>	petrobactin	AsbC	3,4-DHB
Acid-Fast			
<i>M. tuberculosis</i>	mycobactin	MbtA	SAL

<sup>a</sup>SAL, salicylic acid; DHB, 2,3-dihydroxybenzoic acid; 3,4-DHB, 3,4-dihydroxybenzoic acid.

BasE is an aryl acid adenylating enzyme (AAAE) and catalyzes the condensation of DHB **8** with ATP to form an acyl-adenylate intermediate **9**, whereby the carboxy group is activated as a mixed anhydride. Following liberation of pyrophosphate, BasE binds the phosphopantetheinylated aryl carrier protein (ArCP) domain of BasF to form a ternary complex and then catalyzes the transfer of the activated DHB onto the terminal thiol of the pantetheine moiety of BasF to provide thioester **10** (Figure 2).<sup>33</sup> AAAEs are members of the ANL superfamily of enzymes that contain a large N-terminal domain and a smaller C-terminal domain with the active site located at the domain interface.<sup>34</sup> AAAEs thus carry out two reactions, an adenylation and thioesterification, at the same active site. In the adenylation reaction, a catalytic lysine from the C-terminal subdomain coordinates the carboxylate substrate and directs nucleophilic attack on the  $\alpha$ -phosphate of ATP. The enzyme then undergoes a  $\sim 140^\circ$  rigid body rotation about a hinge residue (Lys437 in BasE), which allows the phosphopantetheine arm of the carrier domain to insert into the active site for thioester formation.<sup>34</sup>

5'-O-[*N*-(Salicyl)sulfamoyl]adenosine (Sal-AMS, **12**) and the related 5'-O-[*N*-(2,3-dihydroxybenzoyl)sulfamoyl]adenosine (2,3-DHB-AMS, **13**) are the first confirmed AAAE inhibitors of siderophore biosynthesis with potent nanomolar apparent  $K_i$  values against a range of AAAEs including BasE, YbtE, and MbtA from *A. baumannii*, *Yersinia* sp., and *M. tuberculosis*, respectively (Figure 3).<sup>31,35–37</sup> Sal-AMS and 2,3-DHB-AMS mimic the acyl-adenylate intermediate **9** (Figure 2) through replacement of the labile acylphosphate moiety with



**Figure 3.** Inhibitor and probe structures. 5'-O-[*N*-(Salicyl)sulfamoyl]adenosine (Sal-AMS, **12**), 5'-O-[*N*-(2,3-dihydroxybenzoyl)sulfamoyl]adenosine (2,3-DHB-AMS, **13**), fluorescent probe **14**, and HTS hit 6-phenyl-1-(pyridin-4-ylmethyl)-1H-pyrazolo[3,4-*b*]pyridine-4-carboxylic acid (**15**).

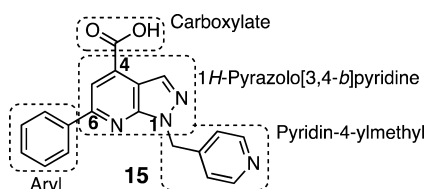
a stable acylsulfamate isostere. Sal-AMS displays impressive activity against the acid-fast Gram-positive *M. tuberculosis* with a minimum inhibitory concentration (MIC) of 0.39  $\mu$ M under iron-deficient conditions. However, the antibacterial potency of Sal-AMS is more than 100 times weaker against Gram-negative *Y. pestis* and *Y. pseudotuberculosis* under the same conditions, despite possessing potent nanomolar enzyme inhibition of YbtE, the respective AAAE from these organisms.<sup>35,38</sup> Moreover, Sal-AMS and 2,3-DHB-AMS display no activity against other Gram-negative organisms including *A. baumannii*, *K. pneumoniae*, *E. coli*, and *P. aeruginosa* (unpublished results, Brian Beck, Laura Celia, ATCC). The reason for such a striking difference could be that the highly polar (ClogP  $\approx -2$ ) and negatively charged nucleoside derivatives may prevent cellular uptake, although many other mechanisms of intrinsic resistance may be involved.

We have recently reported the discovery of a new class of potent non-nucleoside AAAE inhibitors through high-throughput screening (HTS) using a fluorescence polarization (FP) displacement assay with a fluorescent analogue of Sal-AMS (FI-Sal-AMS, **14**) as a ligand.<sup>39</sup> The most potent hit discovered, pyrazolopyridine **15** (Figure 3), binds BasE with a sub-micromolar dissociation constant as determined independently by isothermal titration calorimetry and our FP assay.<sup>39</sup> Further kinetic characterization of **15** reveals that it exhibits competitive inhibition with respect to both substrates 2,3-DHB and ATP.<sup>31</sup> Herein we report the design, synthesis, biochemical, and biological evaluation of a systematic series of analogues of **15** that comprehensively explores the SAR of this promising scaffold. Structural information is also reported for the complexes of BasE with two of the most potent analogues of **15** as well as in vitro data demonstrating that deletion of *basE* in *A. baumannii* impairs growth under iron-deficient conditions.

## RESULTS

**Chemistry.** The structure of 6-phenyl-1-(pyridin-4-ylmethyl)-1H-pyrazolo[3,4-*b*]pyridine-4-carboxylic acid (**15**) discovered from high-throughput screening<sup>39</sup> can be divided into four domains for SAR purposes as depicted in Figure 4. This compound is part of a large compound library supplied by

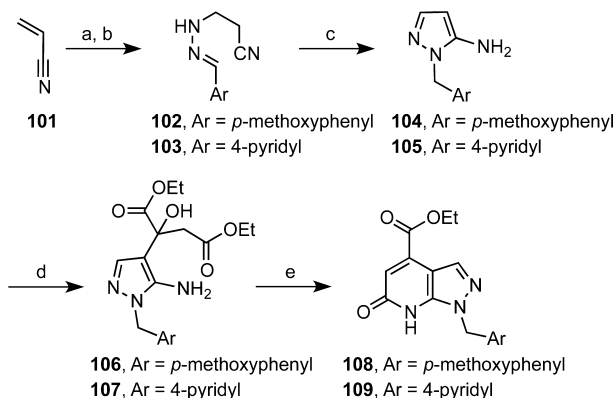
Enamine (Ukraine), and there is no literature available regarding its synthesis or any other properties.



**Figure 4.** Dissection of pyrazolopyridine hit **15** into four domains for SAR analysis.

For the synthesis of **15** and analogues, the key intermediate ethyl 6-oxo-1-(pyridin-4-ylmethyl)-1*H*-pyrazolo[3,4-*b*]-pyridine-4-carboxylate **109** was initially prepared, as well as the *p*-methoxyphenyl (PMP) analogue **108** (Scheme 1). The

**Scheme 1<sup>a</sup>**

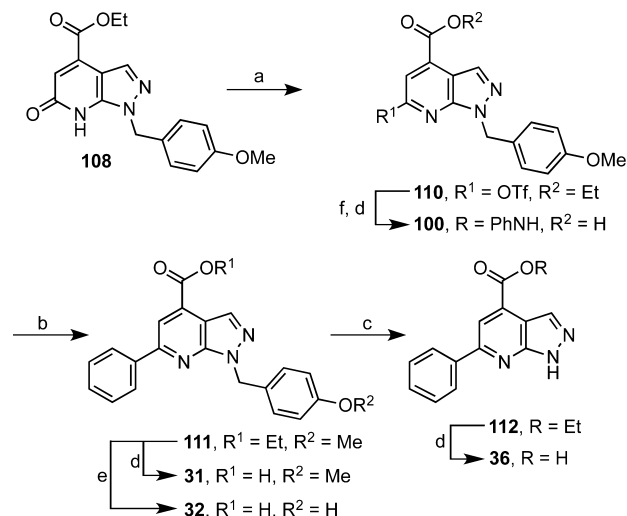


<sup>a</sup>Reaction conditions: (a)  $\text{H}_2\text{NNH}_2 \cdot \text{H}_2\text{O}$ , EtOH, rt, 24 h; (b) ArCHO, 0 °C to rt, 2 h; (c)  $n\text{-BuONa}$ ,  $n\text{-BuOH}$ , 120 °C, 3 h (76%, three steps, from **101**); (d)  $\text{EtO}_2\text{C}(\text{C}=\text{O})\text{CH}_2\text{CO}_2\text{Et}$ , benzene, 65 °C, 20 h, 48–63%; (e) glacial AcOH, reflux, 3 h, 78–81%.

methodology devised by Hohn<sup>40</sup> was used to synthesize the 1-aryl-1*H*-pyrazol-5-amines **104** and **105**, through the multi-component condensation of acrylonitrile **101**, hydrazine, and the appropriate arylaldehydes to afford the intermediate imines **102** and **103**. These were not isolated but directly converted to the corresponding pyrazoles via base-promoted cyclization and subsequent redox isomerization. Pyridone annulation was accomplished in a two-step process involving condensation of **104** and **105** with diethyl oxalacetate to provide **106** and **107**, which were then cyclized to the respective 1*H*-pyrazolo[3,4-*b*]pyridones **108** and **109** by refluxing in glacial acetic acid using the procedure described by Dorn and Müller.<sup>41</sup>

Elaboration of intermediates **108** and **109** to the final C-6 arylpyrazolopyridines requires activation of the tautomerizable pyridone carbonyl as a halide or pseudo-halide followed by Suzuki coupling and ester hydrolysis. We initially began with PMP analogue **108**, since this provides *p*-hydroxybenzyl and *p*-methoxybenzyl analogues **31** and **32**, and selective deprotection of the PMP moiety would allow access to a wide variety of analogues at N-1 by direct alkylation of the resultant free amino group. Chlorination ( $\text{POCl}_3$ ) of **108** was not successful (not shown), but the triflate **110** was readily obtained using triflic anhydride and 2,6-di-*tert*-butyl-4-methylpyridine as base (Scheme 2). Suzuki coupling of **110** with phenylboronic acid

**Scheme 2<sup>a</sup>**



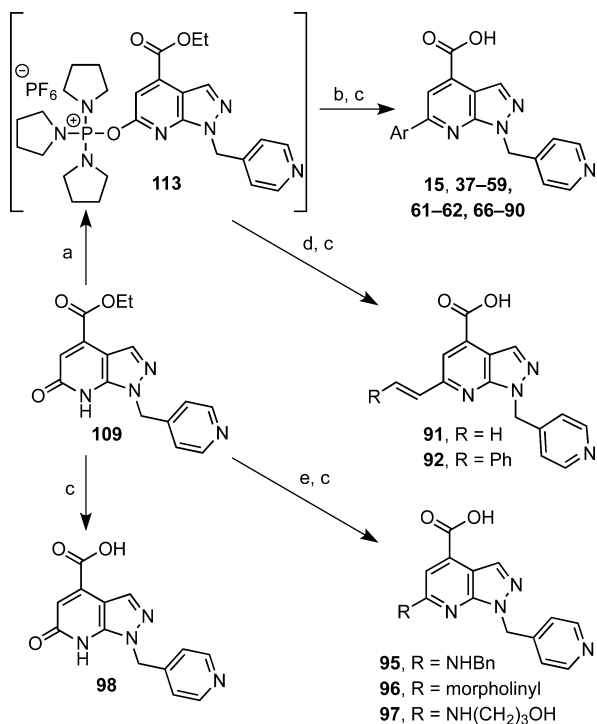
<sup>a</sup>Reaction conditions: (a) 2,6-di-*tert*-butyl-4-methylpyridine,  $\text{TiF}_2\text{O}$ ,  $\text{CH}_2\text{Cl}_2$ , –78 to 0 °C, 4 h, 68%; (b)  $\text{Pd}(\text{PPh}_3)_4$ ,  $\text{Cs}_2\text{CO}_3$ ,  $\text{PhB}(\text{OH})_2$ , dioxane, 100 °C, 5 h, 96%; (c) TFA, 70 °C, 24 h, 85%; (d) aq NaOH, THF, rt, 4 h, 84% (average); (e)  $(\text{CH}_3)_2\text{S} \cdot \text{BF}_3$ , 0 °C to rt, 18 h, 17%; (f)  $\text{Pd}(\text{OAc})_2$ , BINAP,  $\text{Cs}_2\text{CO}_3$ ,  $\text{PhNH}_2$ , dioxane, 100 °C, 22 h, 90%.

under standard conditions furnished the intermediate **111**. Cleavage of the PMP group proceeded optimally in neat TFA at 70 °C to afford compound **112**. Alkylation of **112** with 4-(bromomethyl)pyridine under a variety of conditions was then attempted. Although the desired product **15** was obtained, the reaction was not regioselective and alkylation occurred at both N-1 and N-2 of the pyrazole, leading to poor yields of the desired product (not shown). The intermediates **111** and **112** were readily hydrolyzed with NaOH in THF–H<sub>2</sub>O at room temperature, providing compounds **31** and **36**. The *p*-methoxy group of **111** was hydrolyzed using boron trifluoride–dimethyl sulfate complex, yielding the *p*-hydroxybenzyl analogue **32**. Buchwald–Hartwig coupling of triflate **110** with aniline followed by hydrolysis of the ethyl ester furnished the phenylamino analogue **100**.

To explore the SAR of the 6-aryl domain of the lead compound **15**, we first attempted to prepare the triflate of **109** using the procedure described for PMP analogue **108**. However, triflation was not successful in this case, probably because of the presence of the pyridine moiety. We then explored the conditions developed by Kang and co-workers<sup>42</sup> for the PyBroP-mediated activation of tautomerizable heterocycles. Treatment of **109** with PyBroP at room temperature for 2 h resulted in the formation of the activated intermediate **113** as monitored by mass spectrometry that was not isolated but directed coupled to phenylboronic acid under standard Suzuki conditions to afford the desired product in a respectable 74% yield (Scheme 3). Hydrolysis of the ethyl ester and HPLC purification provided lead compound **15** in 81% yield that possessed identical <sup>1</sup>H NMR, <sup>13</sup>C NMR, and HRMS data compared to the compound obtained from the commercial vendor Enamine. The success of the Kang protocol for activation of **109** highlights the chemoselectivity of PyBroP-mediated activation for highly functionalized heterocycles.

We used parallel synthesis to prepare a systematic series of 54 (hetero)aryl-substituted analogues with substitution at C-6 (Scheme 3). Parallel synthesis was performed on a 0.33 mmol scale employing 100 mg of pyrazolopyridone **109** in 8 mL



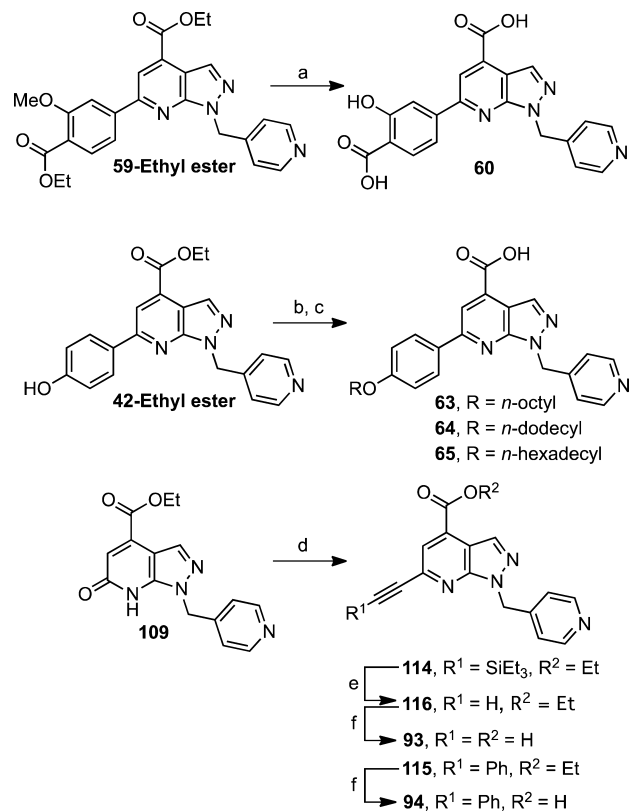
Scheme 3<sup>a</sup>

<sup>a</sup>Reaction conditions: (a) PyBroP, Et<sub>3</sub>N, dioxane, rt, 2 h; (b) ArB(OH)<sub>2</sub> or ArB(OH)<sub>2</sub>-pinacolate ester, PdCl<sub>2</sub>dppf, Na<sub>2</sub>CO<sub>3</sub>, 5:1 dioxane–H<sub>2</sub>O, 100 °C, 4 h, 64% (average, two steps, from **109**); (c) aq. NaOH, THF, rt, 4 h, 80% (average); (d) R–C≡C–B(OH)<sub>2</sub> or respective pinacolate ester, PdCl<sub>2</sub>(PPh<sub>3</sub>)<sub>2</sub>, Na<sub>2</sub>CO<sub>3</sub>, 5:1 dioxane–H<sub>2</sub>O, 100 °C, 4 h, 76–84% (two steps, from **109**); (e) BOP, DBU, HNR<sup>1</sup>R<sup>2</sup>, dioxane, 70 °C, 5 h, 22–79%. The structures of **37–59**, **61**, **62**, and **66–90** are shown in Tables 5 and 6.

sealed vials using a stock solution of all reagents. Extraction of the products from the reaction mixtures was achieved with dichloromethane using phase-separation cartridges. The esters were purified by flash chromatography with an average yield of 64% (range 7–97%), an excellent result considering that a standard purification method was utilized for all compounds. In some cases, when halogenated (hetero)arylboronic acids were used, more than one product was obtained because of a second Suzuki coupling (compounds **73**, **74**, and **85**; Tables 5 and 6). Whenever possible, the two products were isolated. Hydrolysis of the esters was performed with NaOH in THF–H<sub>2</sub>O with good yields, affording compounds **15**, **37–59**, **61**, **62**, and **66–90** (structures in Tables 5 and 6), which were purified by HPLC and lyophilized. The PyBroP-activated intermediate **113** was also used to successfully introduce alkene groups using similar conditions to provide analogues **91** and **92** after ester hydrolysis (Scheme 3).

BOP-mediated coupling of the pyrazolopyridone **109** with three different amines was performed successfully using the procedure developed by Wan et al.,<sup>43</sup> further increasing the scope of this key intermediate and the range of substituents in the pyrazolopyridine at C-6 (Scheme 3). Analogues **95–97** were thus obtained following ester hydrolysis. Simple hydrolysis of the pyrazolopyridone intermediate **109** afforded analogue **98**, which lacks a 6-aryl moiety (Scheme 3).

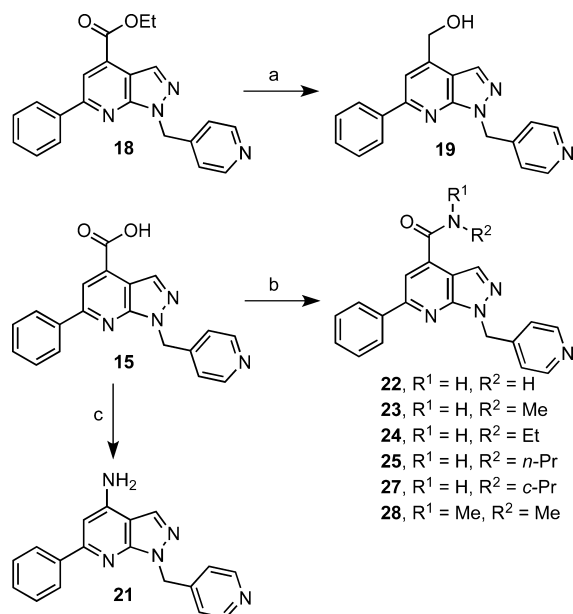
A further series of C-6 substituted analogues was prepared as shown in Scheme 4. Analogue **60** incorporating salicylic acid at C-6 was prepared from **59**-ethyl ester through simultaneous

Scheme 4<sup>a</sup>

<sup>a</sup>Reaction conditions: (a) (CH<sub>3</sub>)<sub>2</sub>S·BF<sub>3</sub>, DCM, 0 °C to rt, 3.5 h, 37%; (b) R–Br, Na<sub>2</sub>CO<sub>3</sub>, dioxane–H<sub>2</sub>O, 80 °C, 12 h; (c) NaOH, MeOH, rt, 2 h, 40–70% (two steps, from **42**-ethyl ester); (d) (i) PyBroP, Et<sub>3</sub>N, dioxane, rt, 2 h; (ii) R–C≡C–H, PdCl<sub>2</sub>(CH<sub>3</sub>CN)<sub>2</sub>, 2-(dicyclohexylphosphino)biphenyl, Cs<sub>2</sub>CO<sub>3</sub>, dioxane–H<sub>2</sub>O, 85 °C, 6 h, 77–87%; (e) TBAF, THF, 0 °C, 3 h, 35%; (f) NaOH, MeOH, rt, 2 h, 41–65%.

cleavage of the methyl ether and ethyl esters by treatment with boron trifluoride–dimethyl sulfate complex. We were also interested in evaluating the impact of increased lipophilicity of the lead compound **15**; hence, a short series of analogues was synthesized bearing a 4-alkoxyphenyl group with 8-, 12-, and 16-carbon linear alkyl chains (compounds **63–65**). This strategy was successful in our previous SAR studies of Sal-AMS (**12**), maintaining or even increasing the respective inhibitory potency against MbtA, the AAAE from *M. tuberculosis*.<sup>44</sup> These compounds were synthesized through alkylation of **42**-ethyl ester with the corresponding alkyl bromides (Scheme 4). The resulting esters were then hydrolyzed with NaOH to afford compounds **63–65**. We also prepared two alkyne analogues by PyBroP activation of **109** and subsequent palladium-catalyzed Sonogashira with triethylsilylacetylene and phenylacetylene under copper-free conditions employing PdCl<sub>2</sub>(CH<sub>3</sub>CN)<sub>2</sub> and Buchwald's 2-(dicyclohexylphosphino)biphenyl ligand to afford **114** and **115** (Scheme 4).<sup>45</sup> Notably, standard Sonogashira conditions did not afford any of the desired product. Deprotection of the terminal TES group in **114** with TBAF furnished **116**. Saponification of **115** and **116** with NaOH in aqueous THF provided **94** and **93**, respectively.

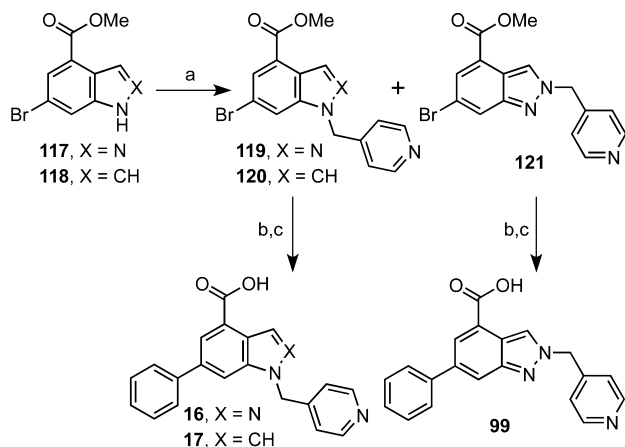
A small series of analogues was prepared as shown in Scheme 5 to study the modification at C-4 of the lead compound **15**. LiAlH<sub>4</sub> reduction of **18** provided hydroxy analogue **19**. Amides

Scheme 5<sup>a</sup>

<sup>a</sup>Reaction conditions: (a) LiAlH<sub>4</sub>, THF, 0 °C to rt, 2 h, 48%; (b) (i) (COCl)<sub>2</sub>, CH<sub>2</sub>Cl<sub>2</sub>, DMF (1 equiv), 0 °C, 1 h; (ii) HNR<sup>1</sup>R<sup>2</sup>, DMAP, rt, 1 h, 39% (average); (c) (i) (COCl)<sub>2</sub>, CH<sub>2</sub>Cl<sub>2</sub>–THF (3:1), rt, 4 h; (ii) NaN<sub>3</sub>, acetone–H<sub>2</sub>O (1:1); (iii) TFA, benzene, reflux, 16 h; (iv) K<sub>2</sub>CO<sub>3</sub>, MeOH, rt, 8 h, 31%.

22–25 and 27–28 were synthesized by conversion of 15 to the corresponding acid chloride, employing oxalyl chloride followed by aminolysis. Functional group interconversion of carboxylic acid 15 to amine 21 was achieved by Curtius rearrangement of the respective acyl azide.

To explore the importance of the N-2 and N-7 atoms of the pyrazolo[3,4-*b*]pyridine scaffold, we prepared analogues 16 and 17 from 6-bromo-1*H*-indazole-4-carboxylate 117 and 6-bromo-1*H*-indole-4-carboxylate 118 (Scheme 6). Alkylation of indazole 117 with 4-(bromomethyl)pyridine hydrobromide employing Cs<sub>2</sub>CO<sub>3</sub> afforded a mixture of regioisomers 119 and 121 in 31% and 19% yield, respectively, favoring the desired N-1 alkylated product. Indole 120 was prepared analogously from

Scheme 6<sup>a</sup>

<sup>a</sup>Reaction conditions: (a) Cs<sub>2</sub>CO<sub>3</sub>, 4-(bromomethyl)pyridine hydrobromide, DMF, rt, 3 h, 50–77%; (b) PdCl<sub>2</sub>dppf, Cs<sub>2</sub>CO<sub>3</sub>, PhB(OH)<sub>2</sub>, dioxane, 100 °C, 5 h, 63–77% (c) aq NaOH, THF, rt, 4 h, 20–77%.

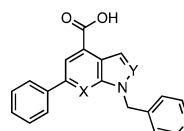
118 in 77% yield. All three compounds were subjected to Suzuki coupling with phenylboronic acid, and the methyl esters were hydrolyzed to provide the final compounds 16, 17, and 99.

**Direct Binding Studies.** The binding of all analogues to BasE was measured using a fluorescence polarization (FP) assay that measures displacement of the active-site directed fluorescent probe Fl-Sal-AMS 14 (see Figure 3) from BasE, which results in a decrease in polarization.<sup>39</sup> Fitting of the resultant displacement curve following the analysis described by Wagner and co-workers enables determination of the ligand dissociation constant.<sup>46</sup> We had previously demonstrated that our direct-binding FP assay agrees closely with results obtained by isothermal titration calorimetry and a functional steady-state kinetic assay that measures acylation of the native aryl-carrier protein domain of BasF.<sup>31</sup> Although this manuscript is primarily focused on *A. baumannii* and inhibition of BasE, we also evaluated all compounds against the homologue MbtA from *M. tuberculosis* as a means to assess inhibitor specificity toward other AAAEs. MbtA was selected, since it is a representative AAAE that utilizes salicylic acid (SAL) instead of 2,3-dihydroxybenzoic acid (DHB) as the native aryl acid substrate.

Direct binding experiments were performed in a 96-well plate format in a 100 μL volume containing 20 nM Fl-Sal-AMS 14 and 200 nM BasE or 50 nM MbtA. Fitting of the experimental data in the form of measured anisotropy (*A*<sub>OBS</sub>) versus test compound concentration (*L*<sub>ST</sub>) to eqs 1 and 2 (see Experimental Section) provided the equilibrium dissociation constant (*K*<sub>D</sub>) for each compound. The *K*<sub>D</sub> of the lead compound 15, previously determined as 78 nM against BasE from a purchased sample,<sup>39</sup> was redetermined here as 36 nM for BasE and 3.7 μM for MbtA for a newly synthesized and purified sample.

The importance of the 1*H*-pyrazolo[3,4-*b*]pyridine scaffold was evaluated with indazole 16 and indole 17 analogues wherein the N-2 and N-7 atoms are replaced with CH isosteres (Table 2). Deletion of N-7 in indazole 16 is well tolerated

Table 2. SAR of the Core Heterocycle

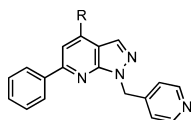


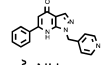
compd	X	Y	<i>K</i> <sub>D</sub> (nM)	
			BasE	MbtA
15	N	N	36.1 ± 4.9	(3.74 ± 0.41) × 10 <sup>3</sup>
16	C	N	84.8 ± 10.0	(27.6 ± 4.2) × 10 <sup>3</sup>
17	C	C	(52.2 ± 4.8) × 10 <sup>3</sup>	(161 ± 7) × 10 <sup>3</sup>

resulting in a 2-fold loss of potency toward BasE. By contrast, removal of N-2 in indole 17 results in a drastic 1400-fold loss of affinity toward BasE. A similar trend for 15–17 was observed for MbtA; however, the relative magnitude differences in binding affinities were different. These results demonstrate that the pyrazole N-2 nitrogen atom is essential while the N-7 nitrogen atom is dispensable for potent activity.

Next, the role of the carboxylic acid at C-4 in 15 was assessed with a series of 12 analogues (Table 3). All modifications to the carboxylic acid lead to a decrease in binding affinity. Deletion of the carboxy group in 20 results in a complete loss of affinity, while ethyl ester 18 is 60-fold less potent. Notably, the neutral

Table 3. SAR at C-4



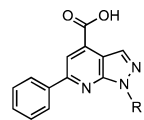
Compound	R	$K_D$ (nM)	
		BasE	MbtA
15	$\text{---COOH}$	$36.1 \pm 4.9$	$(3.74 \pm 0.41) \cdot 10^3$
18	$\text{---COOEt}$	$(2.16 \pm 0.30) \cdot 10^3$	$>100 \cdot 10^3$
19	$\text{---CH}_2\text{OH}$	$102 \pm 8$	$(16.8 \pm 4.0) \cdot 10^3$
20		$>100 \cdot 10^3$	$>100 \cdot 10^3$
21	$\text{---NH}_2$	$200 \pm 25$	$(36.4 \pm 7.2) \cdot 10^3$
22	$\text{---CONH}_2$	$66.8 \pm 7.3$	$(8.57 \pm 0.79) \cdot 10^3$
23	$\text{---CONHMe}$	$420 \pm 54$	$>50 \cdot 10^3$
24	$\text{---CONHEt}$	$908 \pm 69$	$>50 \cdot 10^3$
25	$\text{---CONH}(n\text{-Pr})$	$249 \pm 27$	$>50 \cdot 10^3$
26	$\text{---CONH}(i\text{-Pr})$	$164 \pm 13$	$>100 \cdot 10^3$
27	$\text{---CONH}(c\text{-Pr})$	$150 \pm 19$	$>100 \cdot 10^3$
28	$\text{---CONMe}_2$	$334 \pm 38$	$>50 \cdot 10^3$

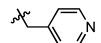
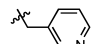
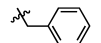
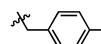
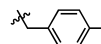
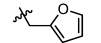
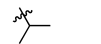
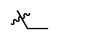
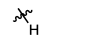
carboxamide **22** and hydroxymethyl **19** are the best tolerated of all modifications, producing a modest 1.8- and 2.8-fold loss in affinities for BasE. In the amide series (compounds **23–28**), substitution of the amide provides a minor-to-modest decrease in potency toward BasE when compared to the carboxamide **22**, varying from 2.2- to 13.6-fold. However, no clear trend in steric or electrostatic interactions is observed. Finally, replacement of the carboxy group with an amino group in **21** is surprisingly well tolerated for BasE, resulting in an approximately 6-fold loss in potency. Collectively, these results suggest that a hydrogen-bond donor at C-4 is required (**18** and **20** vs **19** and **21**), that the electrostatic interaction of the negatively charged carboxylate is not important (**15** vs **22**), and that small alkyl substituents are reasonably tolerated (**25–27**). Similar trends were observed with MbtA except that substituted amides were not accepted.

All modifications performed at N-1 led to either complete loss in affinity or drastic loss of potency against both BasE and MbtA (Table 4). Even a minimal change such as transposition of the pyridine ring nitrogen from the para to the meta position causes complete loss of affinity against both enzymes. The only compound in this series that maintains modest activity (a 15-fold decrease in affinity toward BasE and no activity against MbtA) is *p*-hydroxyphenylmethyl **32**, which possesses a hydrogen-bond acceptor moiety at an equivalent position as the 4-pyridyl substituent in **15**.

Extensive SAR studies were then carried out at C-6 of **15**, as it soon became evident that this was the most amenable to modification. Accordingly, 62 analogues were synthesized, and the respective results are shown in Table 5 for phenyl derivatives and in Table 6 for other analogues including heterocycles, amines, alkenes, and alkynes. The results obtained in this series are quite promising, as there are 16 compounds that improved or equaled the potency of the lead compound **15**, notably compounds **42**, **51**, **67**, and **79**, with  $K_D$  under 10 nM toward BasE. The actual  $K_D$  values for these compounds may be even lower, since these are already at the lower detection limit of the fluorescence polarization assay.

Table 4. SAR at N-1

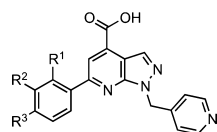


Compound	R	$K_D$ (nM)	
		BasE	MbtA
15		$36.1 \pm 4.9$	$(3.74 \pm 0.41) \cdot 10^3$
29		$>100 \cdot 10^3$	$>100 \cdot 10^3$
30		$>100 \cdot 10^3$	$>100 \cdot 10^3$
31		$>100 \cdot 10^3$	$>100 \cdot 10^3$
32		$556 \pm 66$	$>100 \cdot 10^3$
33		$>100 \cdot 10^3$	$>100 \cdot 10^3$
34		$>500 \cdot 10^3$	$>500 \cdot 10^3$
35		$>500 \cdot 10^3$	$>500 \cdot 10^3$
36		$>100 \cdot 10^3$	$>100 \cdot 10^3$

Thirty-eight analogues (**37–74**) were synthesized in the C-6 phenyl series (Table 5). Unless explicitly stated the SAR refers to BasE and the differences in activity are relative to lead compound **15**. A methyl, hydroxy, and chloro scan of the ortho, meta, and para positions was performed (compounds **37–42** and **44–46**) to assess the ability to tolerate substitution at each position. All substitutions at the ortho position result in a decrease in affinity ranging from 7- to nearly 70-fold. Both *o*-methyl **37** and *o*-chloro **44** possess a drastic loss in affinity (60- to 70-fold), whereas the *o*-hydroxy **40** is only 7-fold less potent, perhaps because of a possible intramolecular H-bond formed with the adjacent pyridine nitrogen, which could stabilize the structure in a favorable conformation. Substitution at both the meta and para positions is better tolerated. While most compounds result in a modest decrease in affinity ranging from 3- to 6-fold, *p*-hydroxy **42** is more than 4-fold more potent than **15**. The observed SAR with respect to MbtA has a nearly identical trend except that *p*-methyl **39** is the most potent toward MbtA with a 2.6-fold increase in affinity.

On the basis of the ability to tolerate substitution at the para position, we prepared a systematic series of 17 analogues with a range of functional groups (**43**, **47–62**). Among this initial series *p*-nitro **51** is the only analogue with substantially improved potency resulting in a 9-fold increase in affinity. Several other analogues including *p*-fluoro **48**, *p*-bromo **47**, *p*-methylthio **61**, *p*-cyano **56**, and *p*-methylsulfonyl **55** possess a modest increase in affinity ranging from 1.3- to 2.8 fold. However, the majority of analogues are less potent resulting in a modest decrease in affinity from 2.2-fold for *p*-amino **52** and *p*-methoxy **62** to over 20-fold for *p*-acetamino **54** and *p*-carboxylate **58**. The combination of a *p*-carboxylate and a *m*-hydroxy in salicylate **60** is only 4.7-fold less potent, showing that the additional *m*-hydroxy is able to partially restore binding affinity. Overall, no clear trends emerged in regard to steric or electronic effects. The SAR of this series with respect to MbtA does not parallel that observed for BasE with *p*-methylsulfonyl **55** displaying the highest affinity (29-fold greater than **15**) and

Table 5. SAR of C-6 Phenyl Group



compd	R <sup>1</sup>	R <sup>2</sup>	R <sup>3</sup>	K <sub>D</sub> (nM)	
				BasE	MbtA
15	H	H	H	36.1 ± 4.9	(3.74 ± 0.41) × 10 <sup>3</sup>
37	Me	H	H	(2.15 ± 0.11) × 10 <sup>3</sup>	>100 × 10 <sup>3</sup>
38	H	Me	H	158 ± 24	(7.40 ± 0.90) × 10 <sup>3</sup>
39	H	H	Me	212 ± 22	(1.44 ± 0.15) × 10 <sup>3</sup>
40	OH	H	H	255 ± 36	(6.50 ± 0.90) × 10 <sup>3</sup>
41	H	OH	H	124 ± 17	(7.67 ± 1.15) × 10 <sup>3</sup>
42	H	H	OH	8.85 ± 3.16	(3.70 ± 0.50) × 10 <sup>3</sup>
43	H	H	CH <sub>2</sub> OH	247 ± 33	(3.70 ± 0.60) × 10 <sup>3</sup>
44	Cl	H	H	(2.48 ± 0.19) × 10 <sup>3</sup>	>100 × 10 <sup>3</sup>
45	H	Cl	H	26.0 ± 4.0	(4.60 ± 0.50) × 10 <sup>3</sup>
46	H	H	Cl	153 ± 21	953 ± 90
47	H	H	Br	20.6 ± 7.0	560 ± 28
48	H	H	F	28 ± 4.7	(1.89 ± 0.21) × 10 <sup>3</sup>
49	F	H	F	42.6 ± 8.3	(8.00 ± 0.90) × 10 <sup>3</sup>
50	H	H	CF <sub>3</sub>	191 ± 27	887 ± 96
51	H	H	NO <sub>2</sub>	3.91 ± 2.27	202 ± 38
52	H	H	NH <sub>2</sub>	78.2 ± 13.2	(4.08 ± 0.63) × 10 <sup>3</sup>
53	H	H	N(Me) <sub>2</sub>	628 ± 98	(1.70 ± 0.30) × 10 <sup>3</sup>
54	H	H	NH(C=O)Me	747 ± 65	(4.20 ± 0.80) × 10 <sup>3</sup>
55	H	H	SO <sub>2</sub> Me	13.0 ± 6.1	130 ± 23
56	H	H	CN	22.7 ± 6.2	380 ± 46
57	H	H	C(=O)NH <sub>2</sub>	288 ± 45	(1.00 ± 0.30) × 10 <sup>3</sup>
58	H	H	COOH	776 ± 119	(6.10 ± 0.80) × 10 <sup>3</sup>
59	H	OMe	COOH	(1.70 ± 0.15) × 10 <sup>3</sup>	(49.9 ± 3.7) × 10 <sup>3</sup>
60	H	OH	COOH	169 ± 13.4	495 ± 34
61	H	H	SMe	23.5 ± 5.5	178 ± 15
62	H	H	OMe	78.2 ± 13.2	(3.23 ± 0.38) × 10 <sup>3</sup>
63	H	H	O(CH <sub>2</sub> ) <sub>7</sub> CH <sub>3</sub>	191 ± 13	>50 × 10 <sup>3</sup>
64	H	H	O(CH <sub>2</sub> ) <sub>11</sub> CH <sub>3</sub>	(28.4 ± 3.9) × 10 <sup>3</sup>	>50 × 10 <sup>3</sup>
65	H	H	O(CH <sub>2</sub> ) <sub>15</sub> CH <sub>3</sub>	n.d. <sup>a</sup>	n.d.
66	H	H	OPh	32.5 ± 6.3	187 ± 28
67	H	H	OCH <sub>3</sub> Ph	2.14 ± 1.46	(5.40 ± 0.90) × 10 <sup>3</sup>
68	H	H	OCH <sub>3</sub> ( <i>p</i> -PhOMe)	44.5 ± 7.7	(5.80 ± 0.90) × 10 <sup>3</sup>
69	H	H	C(=O)Me	104 ± 11	134 ± 22
70	H	H	C(=O)Ph	19.1 ± 4.9	19.1 ± 2.4
71	H	Ph	H	164 ± 20	(3.60 ± 0.38) × 10 <sup>3</sup>
72	H	H	Ph	125 ± 9	(3.50 ± 0.30) × 10 <sup>3</sup>
73	H	H	<i>p</i> -PhBr	181 ± 39	(19.7 ± 0.9) × 10 <sup>3</sup>
74	<i>o</i> -PhCl	H	H	(19.7 ± 0.9) × 10 <sup>3</sup>	>50 × 10 <sup>3</sup>

<sup>a</sup>n.d., not determined due to poor solubility.

*p*-carboxy **58** the lowest affinity (2-fold lower than **15**) among the para-substituted analogues.

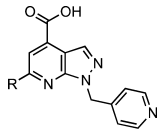
We next explored bulky hydrophobic groups (**63–74**) to define a steric boundary of the active site (Table 5). Long chain alkoxy groups (compounds **63–65**) reduce binding affinity and result in poor solubility (compound **65** was insoluble in the assay conditions). Since the bulky phenyl group in *p*-phenoxy **66** does not adversely affect affinity, we decided to further explore the SAR with other groups and synthesized *p*-biphenyl **72** that is 3.5-fold less potent and *p*-benzoyl **70**, which is 2-fold more potent. Introduction of a CH<sub>2</sub> spacer in *p*-phenoxy **66** provided *p*-benzyloxy **67** that possesses an impressive 17-fold increase in affinity. Further addition of a *p*-methoxy group to **67**

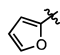
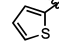
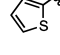
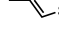


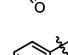
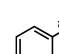
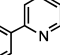
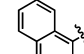
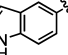
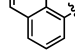
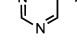
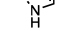



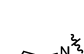
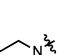
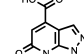

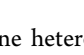
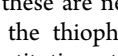
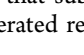
affords 4-methoxybenzyloxy **68** that is 21-fold less potent than **67**. The overall SAR trends for this series of compounds with respect to MbtA do not correlate very closely with BasE. *p*-Benzoyl **70** is the most potent analogue against MbtA with a K<sub>D</sub> of 19 nM, which is an astonishing 197-fold more potent than the lead compound **15**. Among the series of compounds in Table 5, *p*-benzyloxy **67** and *p*-benzoyl **70** emerged as the most attractive because of their high affinities toward BasE. Additionally, **70** was deemed particularly interesting as a result of its balanced activity against both MbtA and BasE.

We also synthesized a series of 24 analogues **75–98** containing a wide variety of heterocycles, alkenes, alkynes, and amines at C-6 (Table 6). The five-membered furan and



Table 6. SAR at C-6: Substitution with Heterocycles, Alkynes, Alkenes, and Amines



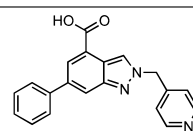
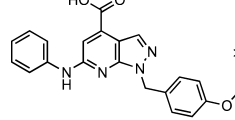
Entry	R	$K_D$ (nM)	
		BasE	MbtA
15	Ph	36.1 ± 4.9	(3.74 ± 0.41)·10 <sup>3</sup>
75		342 ± 53	(19.5 ± 2.2)·10 <sup>3</sup>
76		443 ± 74	(6.68 ± 0.50)·10 <sup>3</sup>
77		340 ± 32	(19.2 ± 1.7)·10 <sup>3</sup>
78		86.9 ± 18.7	(2.54 ± 0.41)·10 <sup>3</sup>
79		7.60 ± 2.49	(2.60 ± 0.60)·10 <sup>3</sup>
80		36.3 ± 7.5	318 ± 56
81		62.4 ± 8.5	701 ± 163
82		39.2 ± 7.5	264 ± 30
83		132 ± 16	(16.8 ± 1.7)·10 <sup>3</sup>
84		121 ± 19	901 ± 109
85		(1.17 ± 0.14)·10 <sup>3</sup>	380 ± 35
86		(7.73 ± 0.43)·10 <sup>3</sup>	> 100·10 <sup>3</sup>
87		61.8 ± 10.4	(2.90 ± 0.20)·10 <sup>3</sup>
88		776 ± 52	(22.5 ± 2.1)·10 <sup>3</sup>
89		583 ± 44	(13.6 ± 0.7)·10 <sup>3</sup>
90		(2.30 ± 0.20)·10 <sup>3</sup>	(27.9 ± 1.6)·10 <sup>3</sup>
91		(1.90 ± 0.20)·10 <sup>3</sup>	> 100·10 <sup>3</sup>
92		280 ± 43	(5.10 ± 0.70)·10 <sup>3</sup>
93		(2.04 ± 0.20)·10 <sup>3</sup>	(18.5 ± 2.0)·10 <sup>3</sup>
94		421 ± 61	(3.00 ± 0.60)·10 <sup>3</sup>
95		(2.32 ± 0.29)·10 <sup>3</sup>	(6.02 ± 0.72)·10 <sup>3</sup>
96		(1.45 ± 0.16)·10 <sup>3</sup>	(29.1 ± 2.0)·10 <sup>3</sup>
97		(2.46 ± 0.24)·10 <sup>3</sup>	(97.7 ± 9.8)·10 <sup>3</sup>
98		> 100·10 <sup>3</sup>	> 100·10 <sup>3</sup>

thiophene heterocycles were initially examined with analogues 75 and 76, and these are nearly 10-fold less potent than 15. A methyl scan in the thiophene ring with compounds 77–79 showed that substitution at positions 3 and 4 (77–78) is not well tolerated resulting in a respective 9- and 2.4-fold decrease

in affinity; however, a 5-fold increase in affinity is conspicuously observed at position 5 (compound 79). Given the enhanced affinity of 5-methyl substituted thiophen-2-yl group, we also evaluated benzothiophene 80, 5-(acetyl)thiophene 81, and 5-(chloro)thiophene 82, but none of these enhance affinity. All of the nitrogen-containing heterocyclic analogues including pyridines 83 and 84, bipyridine 85, isoquinoline 86, indole 87, quinoline 88, pyrimidine 89, and pyrazole 90 result in a loss of potency ranging from 1.7-fold for indole 87 to 215-fold for isoquinoline 86. Similarly, alkene and alkyne analogues 91–94 bind with lower affinities ranging from ~10-fold for phenylethenyl 92 and phenylethynyl 94 to ~55-fold for unsubstituted analogues ethenyl 91 and ethynyl 93. Amino analogues including benzylamine 95, morpholine 96, and 3-hydroxypropylamine 97 are 40-fold to 68-fold less potent. Analogue 98 lacking an aryl moiety at C-6 is completely inactive (>2800-fold less potent). Collectively, the results from this series of analogues demonstrate that a phenyl or isosteric heterocycle is required at C-6 (91, 93, 95–98) and nonpolar heterocycles are optimally tolerated (79, 80, 82 vs 89 and 90). Overall, no improvement in affinity was achieved for 75–98 with BasE. The SAR of this series for MbtA is markedly different, and several compounds were identified that are more potent including benzothiophene 80, 5-(acetyl)thiophene 81, 5-(chloro)thiophene 82, 6-chloropyridine 84, and bipyridine 85, which possess 12-, 5-, 14-, 4-, and 10-fold higher affinities relative to 15.

To complete our cursory SAR studies of 15, we also evaluated two compounds prepared during the course of our studies that involve double modifications (Table 7). Com-

Table 7. Miscellaneous SAR

Compound	$K_D$ (nM)	
	BasE	MbtA
99 	(66.4 ± 6.3)·10 <sup>3</sup>	(58.0 ± 4.1)·10 <sup>3</sup>
100 	> 100·10 <sup>3</sup>	> 100·10 <sup>3</sup>

pound 99 containing an indazole core, but with the (4-pyridyl)methyl group at position 2 instead of position 3, retains some potency toward MbtA (15.5-fold loss) and a pronounced 1800-fold loss in affinity toward BasE. Compound 100 with two unfavorable modifications (replacement of the (4-pyridyl)-methyl group and introduction of an amino group at position 6) displays no affinity toward either BasE or MbtA.

#### Structural Characterization of Inhibitors with BasE.

The active site of BasE, like all AAAE enzymes, contains three subsites that are used to bind the nucleotide, the aromatic acid, and the pantetheine chain of the incoming carrier protein that is used in the thioesterification reaction.<sup>34</sup> The binding pocket for the nucleotide base is bordered on one side by a conserved aromatic residue and on the other by main chain interactions. The aromatic acid binds in a well-defined pocket of the AAAE.<sup>47</sup> Finally, the pantetheine moiety of the cofactor enters the active site through a long tunnel formed between the larger N- and smaller C-terminal domain of the adenylating enzyme.

Table 8. Crystallographic Diffraction and Refinement Data

	BasE-67	BasE-70
PDB accession code	3U16	3U17
resolution (Å)	40.0–2.1	50.0–2.1
space group	$P2_12_12_1$	$P2_12_12_1$
unit cell		
<i>a</i> (Å)	66.1	65.5
<i>b</i> (Å)	144.8	143.3
<i>c</i> (Å)	148.7	148.8
$R_{\text{merge}}^a$ (%)	10.2 (54.2)	7.0 (34.2)
completeness <sup>a</sup> (%)	98.0 (88.4)	90.2 (51.9)
$I/\sigma$ <sup>a</sup>	11.8	10.1
no. observations	365 612	280 779
no. reflections	82 980	74 749
$R_{\text{cryst}}$ (overall/highest resolution shell) <sup>a</sup> (%)	18.5 (26.8)	19.0 (26.7)
$R_{\text{free}}$ (overall/highest resolution shell) <sup>a</sup> (%)	21.9 (31.9)	22.1 (31.0)
Wilson <i>B</i> -factor (Å <sup>2</sup> )	32.1	28.9
average <i>B</i> -factor, protein		
<i>A</i> (Å <sup>2</sup> )	36.6	41.3
<i>B</i> (Å <sup>2</sup> )	36.8	41.2
average <i>B</i> -factor: ligand, solvent, ions (Å <sup>2</sup> )	34.4, 39.9, 46.6	34.9, 41.5, 55.5
no. of water molecules, ions	511 H <sub>2</sub> O, 6 Ca <sup>2+</sup>	379 H <sub>2</sub> O, 1 Ca <sup>2+</sup>
rmsd: bond length (Å), angle (deg)	0.007, 1.06	0.007, 1.05

<sup>a</sup>Values for the highest resolution shell are given in parentheses.

This tunnel forms in the related acyl-CoA synthetases through rotation of the C-terminal domain upon completion of the initial adenylation reaction to form a conformation that is competent for thioester formation.<sup>31</sup>

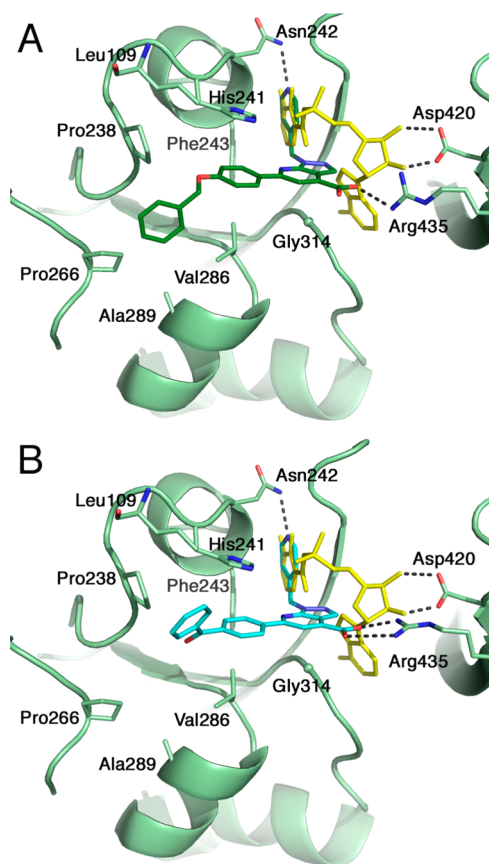
We have previously reported on the crystal structure of BasE bound to DHB-AMS 13, a derivative of 13 bearing an aliphatic chain on the C-2 position of the adenine, and the parent compound 15.<sup>31</sup> The structure of BasE bound to 15 shows that the pyridine approximates the binding mode of the DHB substrate. The nitrogen of the pyridine moiety hydrogen-bonds to the side chain of Asn242, mimicking the binding interaction of the 2- and 3-hydroxy groups of DHB in the structure of BasE bound to 13.<sup>31</sup> Unexpectedly, the binding of 15 did not utilize the carboxylate to mimic the adenylate phosphate or occupy the adenine binding pocket. The phenyl moiety was placed into the pantetheine tunnel. The binding of the phenyl group in this tunnel provides room for the larger inhibitors that were observed to result in higher affinity for BasE. We therefore determined the crystal structure of BasE bound to 67 and 70 to examine how the larger aromatic substituent would fill the pantetheine tunnel.

Crystals of BasE complexes with compounds 67 and 70 diffract well, and the structures were determined by difference Fourier methods. Data collection and refinement statistics are presented in Table 8. As with the previous structures of BasE<sup>31</sup> and other ANL adenyating enzymes,<sup>48,49</sup> the conformationally dynamic C-terminal domain is disordered and is not included in the final models.

The two ligands bind in the active site of BasE in a manner identical to that of 15 reported previously.<sup>31</sup> The pyridin-4-yl-methyl group enters into the DHB binding pocket, forming a hydrogen bond with the side chain of Asn242. This interaction is important for binding, as seen in compounds 29–36 (Table 4) where only compound 32 retained some binding affinity. SAR of the core heterocycle (Table 2) demonstrates the importance of N-2 of the pyrazole ring. The N-2 of the pyrazole ring accepts a hydrogen bond from the main chain amine of

Gly338. Loss of this interaction results in a reduction of affinity of 3 orders of magnitude. This interaction is unique to the HTS ligands, as the amide of Gly338 does not interact with the DHB-AMS analogue of the adenylate 13. In contrast, the N-7 nitrogen of the pyrazolopyridine makes no interactions with the BasE active site residues, and therefore, substitution with a carbon has relatively little impact on binding. The carboxylate groups of 67 and 70 interact with the side chain of Arg435. The interaction of compound 67 with Arg435 is different from that of compounds 15 and 70. However, we note that the electron density for this residue, which is only two residues from the hinge that separates the N-terminal domain from the disordered C-terminal domain, is disordered in one chain in the asymmetric unit for each protein model; therefore, it is likely that Arg435 adopts multiple conformations. Nevertheless, the density is of sufficient quality to be modeled in the second chain in the asymmetric unit for each complex. In the structure of BasE bound to 70, the side chain of Arg435 appears to make a bivalent interaction with the carboxylate. In the model for BasE bound to 67, the side chain of Arg435 interacts with just a single oxygen from the carboxylate. Furthermore, in the previously reported complex with 15, the side chain of Arg435 does not interact directly with the carboxylate of this compound; rather this is mediated through a water molecule. This fact further strengthens our hypothesis of multiple conformations adopted by this residue and could also justify the higher affinity to BasE observed for compounds 67 and 70 (direct interaction between Arg435 and the carboxylate) when compared to 15. SAR with compounds altered in this carboxylate (18–28, Table 3) illustrates a complicated relationship of this group to binding affinity. Replacement of the carboxylate with an alcohol or a carboxamide is reasonably well tolerated in compounds 19 and 22, resulting in only a 3- and 2-fold increase in  $K_D$ . This shows that a strict ionic interaction is not required with the side chain of Arg435.

The longer hydrophobic moieties present in 67 and 70 continue into the pantetheine tunnel (Figure 5). The phenyl



**Figure 5.** Structural characterization of inhibitor binding. Ribbon diagrams are shown for the BasE enzyme bound to (A) inhibitor **67** and (B) inhibitor **70**. Superimposed on both panels is the nucleotide DHB-AMS 13 (yellow) from PDB 3O82, demonstrating the interaction between Asp420 and the ribose hydroxyls and how the pyridyl group of the inhibitors mimics the DHB moiety. Arg435, which is weakly ordered in both chains, interacts with the inhibitor carboxylate. Residues that form the hydrophobic binding pocket are shown in side chain representation.

ring shared by **15**, **67**, and **70** stacks against the side chain of His241. The benzyloxy group of **67** and the benzoyl ring of **70** adopt different conformations. The ring in **67** is positioned closer to the pocket formed by Pro266, Val286, and Ala 289, whereas the ring of **70** is positioned near the top of the groove near residues Leu109 and Pro238. The binding of the phenyl group into this hydrophobic pocket helps to explain the affect of changes at the ortho position in compounds **37** and **44**. The ring is 4.1–4.3 Å from the side chain of Phe243 on one side. The ortho carbon on the other side points toward the location of the disordered C-terminal domain, and we cannot determine if it could be accommodated here. The phenyl ring and the pyrazolopyridine core are nearly coplanar, with interplanar torsion angles ranging from 3° to 15° in the three inhibitor molecules, and the *o*-hydroxy analogue **40** may be tolerated because the hydroxyl could hydrogen-bond with the adjacent N-7 nitrogen from the pyrazolopyridine core.

Interestingly, whereas **70** serves as a potent inhibitor for both BasE and MbtA, **67** serves as a nanomolar inhibitor for BasE but is 1000-fold weaker with MbtA (Table 5). Examination of the binding pockets of the two inhibitor complexes and a sequence alignment of BasE and MbtA shows that the residues labeled in Figure 5 are conserved between BasE and MbtA, with the exception of Pro238 and Ala289, which are replaced by

alanine and leucine, respectively, in MbtA. The replacement of Ala289 with the bulkier leucine is likely the reason that **67** is unable to bind in the same manner as observed in the BasE crystal structure, resulting in the observed micromolar binding constant. We note, however, that the disordered C-terminal domain does form a portion of the pantetheine tunnel in which the aromatic groups bind. Therefore, together with the differences in residues between BasE and MbtA, the C-terminus may also contribute to binding of the inhibitors and be responsible for the different binding affinities observed.

**Antibacterial Activity.** All of the final compounds **15**–**100** were evaluated for antibacterial activity against *A. baumannii* ATCC 19606 under iron-deficient (1 μM FeCl<sub>3</sub> and 200 μM dipyrindyl as chelating agent) and iron-replete conditions (200 μM FeCl<sub>3</sub>) by broth microdilution in M9 minimal medium supplemented with casamino acids (see Experimental Section). However, none of the compounds exhibited antibacterial activity against this bacterium. Several ester intermediates of the most potent inhibitors were also tested to assess whether the higher lipophilicity of these could lead to improved uptake by the bacterium, assuming that a bacterial esterase would hydrolyze the esters. Again, no activity was observed for the esters tested. The resistance of *A. baumannii* to many antibiotics is caused by numerous mechanisms including multidrug efflux pumps and permeability defects due to loss of porins.<sup>50</sup> This could explain the resistance to **15** and its analogues, but further studies are required to assess this hypothesis. A small selection of compounds that exhibited potent activity toward MbtA, namely, **15**, **18**, **66**, **70**, and **82** and their ethyl esters, were also tested against *M. tuberculosis* H37Rv under iron-deficient and iron-replete conditions (Table 9). While some of these compounds displayed very modest

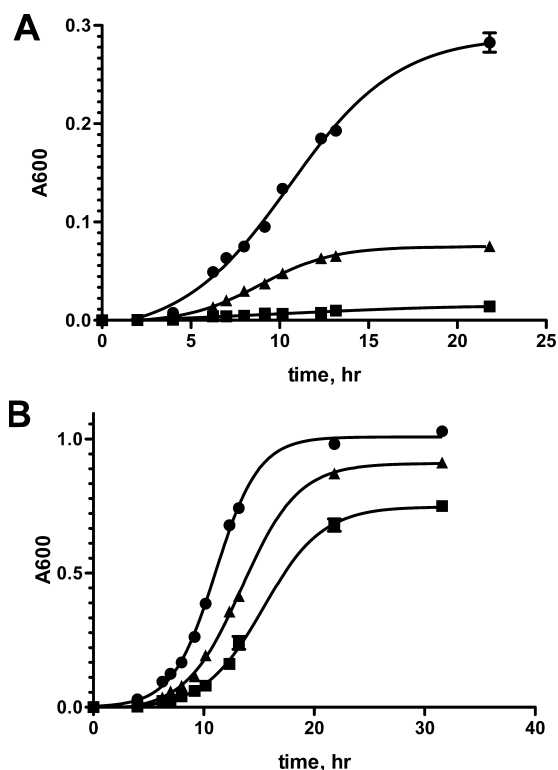
**Table 9.** MIC<sub>99</sub> Determined against *M. tuberculosis* H37Rv (μM)

compd	MIC (μM) iron-deficient (GAST/−Fe)	MIC (μM) iron-replete (GAST/+Fe)
<b>15</b>	>125	>125
<b>18</b>	>125	125
<b>66</b>	25	25
<b>66</b> -ethyl ester	50	100
<b>70</b>	>125	>125
<b>70</b> -ethyl ester	>125	>125
<b>82</b>	50	50
<b>82</b> -ethyl ester	25	25

activity, the activity under iron-replete conditions suggests these compounds may operate by a secondary mechanism of action, since siderophore synthesis in *M. tuberculosis* is dispensable under rich conditions.<sup>22</sup>

**Disruption of BasE in *A. baumannii*.** Earlier studies had rigorously demonstrated the importance of acinetobactin production for growth under iron limiting conditions by insertional inactivation of BasD, the cyclase-condensation didomain NRPS involved in acinetobactin biosynthesis.<sup>27,28</sup> On the basis of our inability to obtain antibacterial activity against *A. baumannii* ATCC 19606, we hypothesized that BasE may be functionally redundant, although no other AAAEs are present in the genome. In order to unequivocally demonstrate the role of BasE in acinetobactin biosynthesis, we deleted *basE* by homologous recombination, replacing it with a kanamycin resistance gene on the chromosome. The deletion was

confirmed by PCR (data not shown). Under iron-deficient conditions,<sup>27</sup> the mutant was severely impaired for growth (Figure 6A). However, under iron-replete conditions,<sup>27</sup> there



**Figure 6.** In vitro growth curves of wild type *A. baumannii* ATCC 19606 (●),  $\Delta basE::kan$  mutant (■), and the  $\Delta basE::kan$  mutant complemented with plasmid pCDD140 (▲). The absorbance at 600 nm is plotted versus incubation time. All strains were inoculated directly into the indicated medium at an  $A_{600}$  of 0.0003 and were not preconditioned under iron limitation. (A) Growth under iron-deficient conditions containing 1  $\mu M$   $FeCl_3$  and 200  $\mu M$  dipyrldyl in M9 minimal medium. All measurements were performed in triplicate, and error bars represent the standard deviation. (B) Growth under iron-rich conditions containing 200  $\mu M$   $FeCl_3$  in M9 minimal medium.

was little observable difference between the growth rates between the wild-type and mutant knockout strain except for a slight increase in lag time for entry in exponential growth (Figure 6B). The modest growth observed for the *basE* mutant in Figure 6A under iron-deficient conditions is caused by residual bacterial iron stores present in the initial inoculum. If the strain is preconditioned under iron-deficient conditions and then inoculated into iron-deficient medium, it is unable to grow. Reintroduction of *basE* on a plasmid was able to partially complement the deletion phenotype (Figure 6A). The inability to fully complement the *basE* knockout strain may be caused by a polar effect on the downstream pathway. The gene immediately downstream of *basE*, *basF*, may be transcriptionally coupled to its upstream neighbor because there are only 18 bp between the two genes and there is no easily recognizable Shine–Dalgarno sequence in this region. Attempts to remove the kanamycin resistance gene and create a clean deletion of *basE* were unsuccessful. In summary, these results in conjunction with prior genetic studies on acinetobactin synthesis suggest that BasE is nonredundant and required for growth of *A. baumannii* under iron-restricted conditions with inorganic iron as the sole source of iron.

## DISCUSSION

The importance of iron for bacterial pathogenesis has led to an increasing interest in targeting iron acquisition pathways for antibacterial development.<sup>51–53</sup> The most ubiquitous strategy employed by bacteria to obtain iron is the synthesis of siderophores.<sup>12</sup> Many bacteria also possess a heme uptake pathway, but this is only important to support bacteremia or bloodstream infections.<sup>54</sup> However, inhibition of siderophore biosynthesis is unlikely to provide broad spectrum antibiotics due to the large number of structurally different siderophores produced by bacteria.<sup>55</sup> Given the alarming rise of antibacterial resistance and the extreme challenges of developing new classes of broad-spectrum agents, the synthesis of narrow spectrum antibiotics is becoming more attractive, particularly for serious infections like *A. baumannii* for which there are few other treatment options.<sup>56</sup>

Collins and co-workers have shown that bactericidal antibiotics generate hydroxyl radicals through the Fenton reaction caused by release of  $Fe^{2+}$  from bacterial iron–sulfur proteins.<sup>23,24</sup> We hypothesize that siderophores may protect bacteria from ROS by chelating free iron. A recent study demonstrated that enterobactin (the prototypical aryl-capped siderophore from *E. coli*) protected this bacteria from oxidative stress.<sup>57</sup> Thus, inhibition of siderophore biosynthesis may have the additional benefit of enhancing the bactericidal activity of existing antibiotics.

Quadri and co-workers were the first to report an inhibitor of siderophore biosynthesis with the synthesis of Sal-AMS, the prototypical AAAE inhibitor.<sup>35–37</sup> Unfortunately, Sal-AMS and related nucleoside analogues have only limited activity against Gram-negative pathogens. We believe this is a result of their highly polar nature and formal negative charge that likely prevents uptake across the negatively charged outer lipopolysaccharide-rich membrane of Gram-negative organisms. The confirmed role of aryl-capped siderophores for virulence in Gram-negative infection including acinetobactin, enterobactin, and yersiniabactin, coupled with lack of activity of Sal-AMS toward *A. baumannii*, *K. pneumoniae*, *P. aeruginosa*, and *E. coli*, motivated us to search for alternative scaffolds as AAAE inhibitors.

We identified pyrazolopyridine **15** using a high-throughput fluorescence polarization assay with BasE from *A. baumannii* and performed detailed SAR studies.<sup>39</sup> The N-2 nitrogen atom of the pyrazolopyridine scaffold **15** is essential, while the N-7 nitrogen is not required for potent activity. Analysis of the cocrystal structures of **15**, **67**, and **70** shows a hydrogen bond between N-2 of the pyrazolopyridine and the amide NH of Gly338 whereas no interaction is observed with N-7. The pyridylmethyl substituent at N-1 is optimal and binds in the DHB pocket with the pyridine substituent occupying a position nearly identical to the native DHB ligand forming a hydrogen bond to Asn242. The importance of this hydrogen bond was assessed by isosteric replacement of the pyridine N with a CH, which resulted in a greater than 2800-fold decrease in binding affinity that corresponds to a staggering loss of more than 4.8 kcal/mol in binding energy. The carboxylate substituent at C-4 is preferred but can be replaced by neutral isosteres such as a carboxamido or hydroxymethyl with only a modest 2- to 3-fold attenuation in potency. Presumably these analogues can maintain the interaction with Arg435 observed with **15**, **67**, and **70**. The phenyl substituent at C-6 is the most tolerant to modification and resulted in the identification of *p*-hydrox-



yphenyl **42**, *p*-nitro **51**, *p*-methylsulfonylphenyl **55**, *p*-benzyloxyphenyl **67**, and *p*-benzophenone **70**, which are up to 18-fold more potent than **15**. Analysis of the cocrystal structures of **67** and **70** reveals that the larger para substituents are accommodated in the pantetheine tunnel. Thus, the pyrazolopyridine analogues are considered multisubstrate inhibitors, since they occupy the binding sites of all three BasE substrates (DHB, ATP, and pantetheine cofactor of BasF).

MbtA was also studied as a representative salicylate adenylating enzyme, which is found in *M. tuberculosis*, *Yersinia* sp., and *K. pneumoniae*. The lead compound **15** and its analogues are generally more active against BasE than MbtA. Benzophenone **70** is the most potent inhibitor of MbtA with a  $K_D$  of 19 nM, a value approximately 200-fold lower than that of the lead compound **15**. Moreover, **70** is equipotent against both MbtA and BasE, demonstrating the feasibility of identifying an inhibitor with balanced activity despite differences in the active-site architecture between these enzymes.

Surprisingly, in spite of the low nanomolar dissociation constants of some of the BasE inhibitors in the biochemical assay, they failed to inhibit growth of *A. baumannii* in vitro. A selection of compounds was also tested against *M. tuberculosis* that encodes for MbtA, a homologue of BasE. Modest bacteriostatic activity was observed with MICs varying between 25 and 100  $\mu$ M. However, the MICs were identical under iron-deficient and iron-replete conditions, indicating that inhibition of MbtA is not fully responsible for the observed activity. Further work will be necessary in order to improve and verify the ability of this series of compounds to penetrate *A. baumannii* and reach their enzyme target BasE as discussed above.

The structure for acinetobactin was described in 1994 as **11** (Figure 2).<sup>25</sup> In 2008 Walsh and Sattely revised the structure of acinetobactin to **1** based on their astute observation of the structural dissimilarities of pseudomonine and acinetobactin despite a common organization of their respective biosynthetic gene clusters.<sup>29,30</sup> The iron-binding properties of acinetobactin have not been evaluated, but it is expected to possess a substantially lower affinity for Fe<sup>3+</sup> than pre-acinetobactin, which contains an oxazoline and hydroxamate functions. In acinetobactin these functional groups rapidly rearrange ( $t_{1/2} \approx 1$  h) to provide the isoxazolidinone in **1** (Figure 2). The revised structure **1** has been confirmed via total synthesis.<sup>26</sup>

The importance of acinetobactin for iron acquisition was first studied in *A. baumannii* strain ATCC 19606.<sup>27,28,58</sup> Insertional inactivation of *basD*, which encodes for a didomain protein responsible for the condensation of the DHB and L-Thr building blocks in acinetobactin biosynthesis, results in a strain incapable of producing acinetobactin.<sup>28</sup> The *basD* knockout is impaired in the ability to replicate under iron-deficient conditions,<sup>27</sup> in human AS49 alveolar epithelial cells,<sup>59</sup> and in a mouse sepsis model.<sup>60</sup> While these studies clearly demonstrate the importance of *basD* for virulence, we wished to confirm that *basE* also phenocopies the *basD* mutant, since these isogenic mutants will potentially produce different siderophore intermediates that may partially rescue loss of acinetobactin. In this study we examined the importance of *basE* for virulence of *A. baumannii* strain ATCC 19606. Deletion of *basE* results in a strain unable to replicate under iron-deficient conditions but that grows at the same rate as the wild-type strain under iron-replete conditions. These results confirm BasE as a valid target and suggest that the inability of

the pyrazolopyridine inhibitors to exhibit whole-cell activity toward *A. baumannii* is due to other factors such as limited accumulation and/or lack of vulnerability of BasE to inhibition by small molecules. Vulnerability or amount that a target must be inhibited is another important consideration that cannot be assessed by a simple knockout strain.

The initial studies of iron acquisition in *A. baumannii* focused on strain ATCC 19606 and demonstrated that acinetobactin is the only siderophore produced by this organism.<sup>25</sup> Genome sequencing of the related strain *A. baumannii* ATCC 17978 reveals that it encodes for an additional siderophore pathway of an uncharacterized aryl-capped siderophore.<sup>16</sup> As a result, acinetobactin is dispensable in ATCC 17978.<sup>16</sup> Analysis of the second siderophore gene cluster shows that it encodes for two 2,3-dihydroxybenzoate-AMP ligases (A1S\_2573 and A1S\_2574), which we expect can also be inhibited by our pyrazolopyridine BasE inhibitors.<sup>59,61,62</sup> Comparative genomics studies of six fully sequenced *A. baumannii* strains and PCR analysis of 50 clinical isolates were recently described providing the most detailed picture yet reported of iron acquisition systems in this pathogen.<sup>62</sup> The acinetobactin gene cluster is highly conserved among clinical isolates. Another prevalent gene cluster was identified, which encodes for a putative hydroxamate siderophore. Genes for ferrous uptake and heme uptake are also observed in virtually all strains. The importance of these multiple iron acquisition systems for virulence remains to be evaluated but suggests that this pathogen is capable of using alternative iron sources for survival under different environmental conditions.

## CONCLUSION

A comprehensive analysis of the structure–activity relationships of the HTS hit **15** was performed that examined the importance of the pyrazolopyridine heterocycle, the 4-pyridylmethyl substituent at N-1, the carboxylic acid at C-4, and the phenyl group at C-6 for binding to BasE and MbtA. BasE from *A. baumannii* was the primary focus of the work, and the initial SAR studies defined the crucial interactions necessary to maintain potency and also identified sites amenable to modification. The pyrazolopyridine heterocycle ideally positions the N-1, C-4, and C-6 substituents into the DHB, ATP, and pantetheine binding pockets. The N-2 nitrogen of the pyrazolopyridine forms a key hydrogen bond with the amide backbone of Gly338, but N-7 is dispensable for potent activity. The pyridylmethyl substituent at N-1 is crucial, illustrated by the almost 5 kcal/mol loss in binding affinity by simple deletion of the nitrogen atom in the pyridine. The carboxylic acid at C-4 is not required and can be replaced with alternative hydrogen-bond-acceptor moieties including hydroxymethyl and carbox-amido with only a modest attenuation in binding affinity, demonstrating that the ionic interaction observed between the carboxylic acid and Arg435 in the cocrystal structures of BasE with three different pyrazolopyridine ligands is not critical. The C-6 phenyl group is most tolerant to substitution, and hydrophobic (hetero)aryl substituents are preferred. *p*-Benzyloxyphenyl **67** was identified as the most potent analogue toward BasE with a  $K_D$  of 2 nM. The entire compound series was also evaluated against MbtA, a representative AAAE that activates salicylic acid, and similar SAR trends were observed. HTS hit **15** is considerably less potent toward MbtA with a  $K_D$  of only 3.7  $\mu$ M. However, benzophenone **70** was found to have balanced activity against both BasE and MbtA with a  $K_D$  of 19 nM, which represents a nearly 200-fold increase in potency

toward MbtA. The SAR and structural characterization of ligands with BasE described herein provide a foundation for future studies to improve upon the antibacterial activity and exploit the unique multisubstrate modality of inhibition.

## EXPERIMENTAL SECTION

**Chemistry: General Methods and Materials.** All commercial reagents (Sigma-Aldrich, Acros, Alfa-Aesar) were used as provided. Boronic acids and boronic acid pinacolate esters were purchased from Aldrich, Boron Molecular (Research Triangle, NC), and Frontier Scientific (Logan, UT). Compounds **20**, **26**, **29**, **30**, and **33–35** were purchased from Enamine (Ukraine). Compounds **117** and **118** were obtained from Sinova (Bethesda, MD). Compounds **104**,<sup>63</sup> **114**,<sup>45</sup> and **115**<sup>45</sup> were prepared according to the respective literature procedure. Purity ( $\geq 95\%$ ) of all final compounds was confirmed by reverse-phase HPLC using the indicated method (see Supporting Information). An anhydrous solvent dispensing system (JC Meyer, Laguna Beach, CA) using two packed columns of neutral alumina was used for drying THF, DMF, and  $\text{CH}_2\text{Cl}_2$ , and the solvents were dispensed under argon. All reactions were performed under an inert atmosphere of dry Ar or  $\text{N}_2$  in oven-dried ( $150^\circ\text{C}$ ) glassware. Flash chromatography was performed with an ISCO Combiflash Companion purification system with prepacked silica gel cartridges supplied by Luknova, with the indicated solvent system. Preparative HPLC was performed on a Varian Microsorb MV 100-8 C18 column ( $41.4\text{ mm} \times 250\text{ mm}$ ,  $8\text{ }\mu\text{m}$  particle size) operating at  $40\text{ mL/min}$  with detection at  $254\text{ nm}$  in the conditions described in the Supporting Information.  $^1\text{H}$  and  $^{13}\text{C}$  NMR spectra were recorded on either a Varian 600 MHz or Bruker Avance 400 MHz spectrometer. Proton chemical shifts are reported in ppm from an internal standard of residual chloroform ( $7.26\text{ ppm}$ ), dimethylsulfoxide ( $2.50\text{ ppm}$ ), or methanol ( $3.31\text{ ppm}$ ), and carbon chemical shifts are reported using an internal standard of residual chloroform ( $77.1\text{ ppm}$ ), dimethylsulfoxide ( $39.5\text{ ppm}$ ), or methanol ( $49.0\text{ ppm}$ ). Proton chemical data are reported as follows: chemical shift, multiplicity (s = singlet, d = doublet, t = triplet, q = quartet, p = pentet, m = multiplet, br = broad, ovlp = overlapping), coupling constant, and integration. High-resolution mass spectra were obtained on an Agilent TOF II TOF/MS instrument equipped with an ESI interface.

**Compounds from Scheme 1.** *Diethyl 2-(5-Amino-1-(4-methoxybenzyl)-1H-pyrazol-4-yl)-2-hydroxysuccinate (106)*. A solution of diethyl oxalacetate ( $3.46\text{ g}$ ,  $18.4\text{ mmol}$ ,  $1.01\text{ equiv}$ ) and **104**<sup>63</sup> ( $3.7\text{ g}$ ,  $18.2\text{ mmol}$ ,  $1.0\text{ equiv}$ ) in benzene ( $40\text{ mL}$ ) was heated at  $65^\circ\text{C}$  for  $20\text{ h}$ . The mixture was concentrated, and purification by flash chromatography (3:2 hexanes/EtOAc) afforded the title compound ( $4.5\text{ g}$ ,  $63\%$ ) as a yellow oil:  $R_f = 0.65$  (EtOAc);  $^1\text{H}$  NMR ( $600\text{ MHz}$ ,  $\text{CDCl}_3$ )  $\delta$  1.23–1.27 (m, 6H), 2.92 (d,  $J = 16.8\text{ Hz}$ , 1H), 3.32 (d,  $J = 16.8\text{ Hz}$ , 1H), 3.78 (s, 3H), 4.08 (br s, 2H,  $\text{NH}_2$ ), 4.16 (q,  $J = 7.2\text{ Hz}$ , 2H), 4.24 (q,  $J = 7.2\text{ Hz}$ , 2H), 5.06 (s, 2H), 6.85 (d,  $J = 8.4\text{ Hz}$ , 2H), 7.10 (d,  $J = 8.4\text{ Hz}$ , 2H), 7.23 (s, 1H);  $^{13}\text{C}$  NMR ( $150\text{ MHz}$ ,  $\text{CDCl}_3$ )  $\delta$  14.17, 14.23, 43.9, 51.5, 55.4, 61.2, 62.4, 73.3, 102.7, 114.5, 128.1, 128.5, 135.8, 143.3, 159.4, 171.3, 173.5; HRMS (ESI+) calcd for  $\text{C}_{19}\text{H}_{26}\text{N}_3\text{O}_6$  [ $\text{M} + \text{H}$ ] $^+$  392.1816, found 392.1825 (error 2.3 ppm).

*Ethyl 1-(4-Methoxybenzyl)-6-oxo-6,7-dihydro-1H-pyrazolo[3,4-b]pyridine-4-carboxylate (108)*. A suspension of **106** ( $5.2\text{ g}$ ,  $13.2\text{ mmol}$ ) in glacial acetic acid ( $40\text{ mL}$ ) was refluxed for  $3\text{ h}$ . The mixture was concentrated to approximately half of the volume. Then isopropanol ( $100\text{ mL}$ ) was added and the solution was cooled to room temperature. The product crystallized as a white solid ( $3.5\text{ g}$ ,  $81\%$ ): mp  $235\text{--}236^\circ\text{C}$ ;  $R_f = 0.65$  (1:1 EtOAc/hexane);  $^1\text{H}$  NMR ( $600\text{ MHz}$ ,  $\text{DMSO}-d_6$ )  $\delta$  1.37 (t,  $J = 7.2\text{ Hz}$ , 3H), 3.70 (s, 3H), 4.40 (q,  $J = 7.2\text{ Hz}$ , 2H), 5.46 (s, 2H), 6.86 (d,  $J = 8.4\text{ Hz}$ , 2H), 6.95 (br s, 1H), 7.16 (d,  $J = 8.4\text{ Hz}$ , 2H), 8.11 (s, 1H), 12.05 (br s,  $\text{D}_2\text{O}$ -exchangeable, 1H);  $^{13}\text{C}$  NMR ( $150\text{ MHz}$ ,  $\text{DMSO}-d_6$ )  $\delta$  14.0, 49.5, 55.1, 61.7, 113.9, 128.7, 129.1, 133.0, 134.0, 158.7, 163.5, 164.2 (unable to observe three carbons, estimated at 99, 135, and 147 ppm due to quadrupolar coupling with nitrogen); HRMS (ESI+) calcd for  $\text{C}_{19}\text{H}_{26}\text{N}_3\text{O}_6$  [ $\text{M} + \text{H}$ ] $^+$  328.1292, found 328.1303 (error 3.4 ppm).

*1-(Pyridin-4-ylmethyl)-1H-pyrazol-5-amine (105)*. To a solution of acrylonitrile ( $4.42\text{ g}$ ,  $83\text{ mmol}$ ,  $1.05\text{ equiv}$ ) at  $0^\circ\text{C}$  in absolute EtOH ( $80\text{ mL}$ ) was added hydrazine hydrate ( $3.93\text{ g}$ ,  $79\text{ mmol}$ ,  $1.0\text{ equiv}$ ) dropwise with vigorous stirring over  $10\text{ min}$ . The ice bath was removed, and the mixture was stirred for  $24\text{ h}$  at room temperature. The reaction mixture was cooled to  $0^\circ\text{C}$ . 4-Pyridinecarboxaldehyde ( $8.8\text{ g}$ ,  $82\text{ mmol}$ ,  $1.04\text{ equiv}$ ) was slowly added, and stirring continued for  $2\text{ h}$  at room temperature. The mixture was concentrated. The residue was dissolved in dry *n*-butanol ( $30\text{ mL}$ ), and a  $16\%$  sodium *n*-butoxide solution in *n*-butanol ( $100\text{ mL}$ ,  $167\text{ mmol}$ ,  $2.1\text{ equiv}$ ) was added. The resulting solution was refluxed for  $1\text{ h}$ , cooled to room temperature, and concentrated. The residue was partitioned between  $\text{H}_2\text{O}$  ( $150\text{ mL}$ ) and EtOAc ( $3 \times 150\text{ mL}$ ). The combined organic layers were dried ( $\text{MgSO}_4$ ) and concentrated to afford the title compound ( $10.6\text{ g}$ ,  $76\%$ ) as a pale brown solid:  $R_f = 0.19$  (9:1 EtOAc/MeOH);  $^1\text{H}$  NMR ( $600\text{ MHz}$ ,  $\text{CDCl}_3$ )  $\delta$  3.43 (br s, 2H,  $\text{NH}_2$ ), 5.20 (s, 2H), 5.63 (d,  $J = 1.8\text{ Hz}$ , 1H), 7.00 (d,  $J = 6.0\text{ Hz}$ , 2H), 7.35 (d,  $J = 1.8\text{ Hz}$ , 1H), 8.54 (d,  $J = 6.0\text{ Hz}$ , 2H);  $^{13}\text{C}$  NMR ( $150\text{ MHz}$ ,  $\text{CDCl}_3$ )  $\delta$  50.3, 92.8, 121.7, 139.5, 144.6, 146.0, 150.4; HRMS (ESI+) calcd for  $\text{C}_9\text{H}_{11}\text{N}_4$  [ $\text{M} + \text{H}$ ] $^+$  175.0978, found 175.0976 (error 1.1 ppm).

*Diethyl 2-(5-Amino-1-(pyridin-4-ylmethyl)-1H-pyrazol-4-yl)-2-hydroxysuccinate (107)*. A solution of diethyl oxalacetate ( $10.6\text{ g}$ ,  $56.1\text{ mmol}$ ,  $1.2\text{ equiv}$ ) and **105** ( $8.1\text{ g}$ ,  $46.7\text{ mmol}$ ,  $1.0\text{ equiv}$ ) in benzene ( $100\text{ mL}$ ) was heated at  $65^\circ\text{C}$  for  $15\text{ h}$ . The mixture was concentrated and the residue was recrystallized from EtOH/Et $_2\text{O}$  to afford the title compound ( $10.6\text{ g}$ ,  $48\%$ ) as a pale yellow solid: mp  $118\text{--}120^\circ\text{C}$ ;  $R_f = 0.61$  (7:3 EtOAc/MeOH);  $^1\text{H}$  NMR ( $600\text{ MHz}$ ,  $\text{CDCl}_3$ )  $\delta$  1.27 (ovlp t,  $J = 7.2\text{ Hz}$ , 3H), 1.28 (ovlp t,  $J = 7.2\text{ Hz}$ , 3H), 2.95 (d,  $J = 16.8\text{ Hz}$ , 1H), 3.35 (d,  $J = 16.8\text{ Hz}$ , 1H), 4.16 (br s, 2H,  $\text{NH}_2$ ), 4.19 (q,  $J = 7.2\text{ Hz}$ , 2H), 4.26 (q,  $J = 7.2\text{ Hz}$ , 2H), 5.13 (s, 2H), 7.01 (d,  $J = 6.0\text{ Hz}$ , 2H), 7.29 (s, 1H), 8.55 (d,  $J = 6.0\text{ Hz}$ , 2H);  $^{13}\text{C}$  NMR ( $150\text{ MHz}$ ,  $\text{CDCl}_3$ )  $\delta$  14.20, 14.25, 43.9, 50.4, 61.3, 62.5, 73.3, 103.2, 121.8, 136.8, 143.6, 145.5, 150.4, 171.3, 173.4; HRMS (ESI+) calcd for  $\text{C}_{17}\text{H}_{23}\text{N}_4\text{O}_5$  [ $\text{M} + \text{H}$ ] $^+$  363.1663, found 363.1668 (error 1.4 ppm).

*Ethyl 6-Oxo-1-(pyridin-4-ylmethyl)-6,7-dihydro-1H-pyrazolo[3,4-b]pyridine-4-carboxylate (109)*. A suspension of **107** ( $9.7\text{ g}$ ,  $26.9\text{ mmol}$ ) in glacial acetic acid ( $60\text{ mL}$ ) was refluxed for  $4\text{ h}$ . The mixture was concentrated, and the residue was triturated with isopropanol ( $100\text{ mL}$ ). The white solid that formed was filtered, washed with isopropanol/ether, and dried under vacuum to afford the title compound ( $6.29\text{ g}$ ,  $78\%$ ) as an off-white solid:  $R_f = 0.25$  (9:1 EtOAc/MeOH);  $^1\text{H}$  NMR ( $600\text{ MHz}$ ,  $\text{DMSO}-d_6$ )  $\delta$  1.39 (t,  $J = 7.2\text{ Hz}$ , 3H), 4.42 (q,  $J = 7.2\text{ Hz}$ , 2H), 5.61 (s, 2H), 7.00 (br s, 1H), 7.07 (d,  $J = 6.0\text{ Hz}$ , 2H), 8.20 (s, 1H), 8.49 (d,  $J = 6.0\text{ Hz}$ , 2H), 12.10 (br s, 1H);  $^{13}\text{C}$  NMR ( $150\text{ MHz}$ ,  $\text{DMSO}-d_6$ )  $\delta$  14.0, 49.0, 61.7, 106.4, 109.0, 121.8, 133.6, 134.1, 146.1, 149.8, 163.8, 164.1 (missing 1 C); HRMS (ESI+) calcd for  $\text{C}_{15}\text{H}_{15}\text{N}_4\text{O}_3$  [ $\text{M} + \text{H}$ ] $^+$  299.1139, found 299.1128 (error 3.7 ppm).

**Compounds from Scheme 2.** *Ethyl 1-(4-Methoxybenzyl)-6-(trifluoromethylsulfonyloxy)-1H-pyrazolo[3,4-b]pyridine-4-carboxylate (110)*. To a solution of **108** ( $3.38\text{ g}$ ,  $10.3\text{ mmol}$ ,  $1.0\text{ equiv}$ ) and 2,6-di-*tert*-butyl-4-methylpyridine ( $3.18\text{ g}$ ,  $15.5\text{ mmol}$ ,  $1.5\text{ equiv}$ ) in  $\text{CH}_2\text{Cl}_2$  ( $50\text{ mL}$ ) at  $-78^\circ\text{C}$  was added dropwise a solution of trifluoromethanesulfonic anhydride ( $2.98\text{ mL}$ ,  $17.7\text{ mmol}$ ,  $1.7\text{ equiv}$ ) in  $\text{CH}_2\text{Cl}_2$  ( $10\text{ mL}$ ). The reaction mixture was stirred at  $0^\circ\text{C}$  for  $4\text{ h}$ . The solvent volume was reduced to one-third in vacuo and diluted with EtOAc ( $40\text{ mL}$ ). The resulting solution was washed consecutively with saturated aqueous  $\text{NaHCO}_3$  ( $3 \times 20\text{ mL}$ ),  $\text{H}_2\text{O}$  ( $20\text{ mL}$ ),  $1\text{ M}$  aqueous HCl ( $3 \times 20\text{ mL}$ ),  $\text{H}_2\text{O}$  ( $20\text{ mL}$ ), and saturated aqueous NaCl ( $20\text{ mL}$ ). The organic layer was dried ( $\text{MgSO}_4$ ) and concentrated. Purification by flash chromatography (4:1 hexane/EtOAc) afforded the title compound ( $3.2\text{ g}$ ,  $68\%$ ) as a white solid:  $R_f = 0.43$  (4:1 hexane/EtOAc);  $^1\text{H}$  NMR ( $600\text{ MHz}$ ,  $\text{CDCl}_3$ )  $\delta$  1.48 (t,  $J = 7.2\text{ Hz}$ , 3H), 3.76 (s, 3H), 4.52 (q,  $J = 7.2\text{ Hz}$ , 2H), 5.59 (s, 2H), 6.84 (d,  $J = 8.4\text{ Hz}$ , 2H), 7.37 (d,  $J = 8.4\text{ Hz}$ , 2H), 7.56 (s, 1H), 8.46 (s, 1H);  $^{13}\text{C}$  NMR ( $150\text{ MHz}$ ,  $\text{CDCl}_3$ )  $\delta$  14.3, 51.3, 55.3, 62.7, 109.1, 113.7, 114.2, 118.8 (q,  $^1J_{\text{C-F}} = 319\text{ Hz}$ ,  $\text{CF}_3$ ), 128.0, 130.0, 133.8, 136.3, 148.3, 154.5, 159.7, 163.4; HRMS (ESI+) calcd for  $\text{C}_{18}\text{H}_{17}\text{F}_3\text{N}_3\text{O}_6\text{S}$  [ $\text{M} + \text{H}$ ] $^+$  460.0785, found 460.0762 (error 5.0 ppm).



**Ethyl 1-(4-Methoxybenzyl)-6-phenyl-1H-pyrazolo[3,4-b]pyridine-4-carboxylate (111).** A mixture of **110** (0.50 g, 1.08 mmol, 1.0 equiv), Pd(PPh<sub>3</sub>)<sub>4</sub> (62.5 mg, 0.054 mmol, 0.05 equiv), Cs<sub>2</sub>CO<sub>3</sub> (0.704 g, 2.16 mmol, 2.0 equiv), PhB(OH)<sub>2</sub> (0.198 g, 1.62 mmol, 1.5 equiv), and dioxane (20 mL) was stirred at 100 °C for 5 h. The reaction mixture was cooled to room temperature, filtered through a plug of Celite, and concentrated. Purification by flash chromatography (7:3 hexanes/EtOAc) afforded the title compound (0.39 g, 96%) as a white solid: *R*<sub>f</sub> = 0.49 (7:3 hexanes/EtOAc); <sup>1</sup>H NMR (600 MHz, CDCl<sub>3</sub>) δ 1.50 (t, *J* = 7.2 Hz, 3H), 3.76 (s, 3H), 4.53 (q, *J* = 7.2 Hz, 2H), 5.74 (s, 2H), 6.84 (d, *J* = 9.0 Hz, 2H), 7.40 (d, *J* = 9.0 Hz, 2H), 7.49 (t, *J* = 7.2 Hz, 1H), 7.55 (t, *J* = 7.2 Hz, 2H), 8.22 (d, *J* = 7.2 Hz, 2H), 8.25 (s, 1H), 8.39 (s, 1H); <sup>13</sup>C NMR (150 MHz, CDCl<sub>3</sub>) δ 14.5, 50.6, 55.3, 62.0, 112.1, 114.1, 115.4, 127.7, 129.0, 129.3, 129.8, 129.9, 132.0, 133.2, 138.6, 151.6, 156.9, 159.4, 165.4; HRMS (ESI+) calcd for C<sub>23</sub>H<sub>22</sub>N<sub>3</sub>O<sub>3</sub> [M + H]<sup>+</sup> 388.1656, found 388.1666 (error 2.6 ppm).

**1-(4-Methoxybenzyl)-6-phenyl-1H-pyrazolo[3,4-b]pyridine-4-carboxylic Acid (31).** To a solution of **111** (25 mg, 0.065 mmol) in THF (1 mL) was added 1 N aqueous NaOH (2 mL). The resulting solution was stirred at room temperature for 3 h. The solvent was partially evaporated, the reaction mixture diluted with H<sub>2</sub>O (10 mL) and the pH adjusted to 4–5 with 1 N aqueous HCl. The resulting suspension was extracted with EtOAc (3 × 15 mL). The combined organic layers were washed with saturated aqueous NaCl, dried (MgSO<sub>4</sub>), and concentrated to afford the title compound (23 mg, 98%) as a white solid: <sup>1</sup>H NMR (600 MHz, DMSO-*d*<sub>6</sub>) δ 3.69 (s, 3H), 5.71 (s, 2H), 6.88 (d, *J* = 9.0 Hz, 2H), 7.31 (d, *J* = 9.0 Hz, 2H), 7.53 (t, *J* = 7.2 Hz, 1H), 7.58 (t, *J* = 7.2 Hz, 2H), 8.21 (s, 1H), 8.27 (d, *J* = 7.2 Hz, 2H), 8.37 (s, 1H); <sup>13</sup>C NMR (150 MHz, DMSO-*d*<sub>6</sub>) δ 49.8, 55.0, 111.9, 113.9, 114.7, 127.3, 129.06, 129.18, 129.25, 130.0, 132.5, 133.3, 137.8, 150.9, 155.9, 158.7, 166.0; HRMS (ESI-) calcd for C<sub>21</sub>H<sub>16</sub>N<sub>3</sub>O<sub>3</sub> [M - H]<sup>-</sup> 358.1197, found 358.1200 (error 0.8 ppm).

**1-(4-Hydroxybenzyl)-6-phenyl-1H-pyrazolo[3,4-b]pyridine-4-carboxylic Acid (32).** To a solution of **111** (20 mg, 0.052 mmol, 1.0 equiv) in CH<sub>2</sub>Cl<sub>2</sub> (2 mL) was added dropwise neat boron trifluoride-dimethylsulfide complex (55 μL, 0.052 mmol, 1.0 equiv) at 0 °C. Then the mixture was stirred at room temperature for 18 h. The reaction mixture was slowly poured over ice cold 0.5 M aqueous HCl (10 mL) and extracted with EtOAc (3 × 20 mL). The combined organic layers were washed with saturated aqueous NaHCO<sub>3</sub> (10 mL), H<sub>2</sub>O (10 mL), saturated aqueous NaCl (10 mL), dried (MgSO<sub>4</sub>), and concentrated. The residue was dissolved in THF (1.0 mL). Then 1 N aqueous NaOH (1.0 mL) was added, and the resulting solution was stirred at room temperature for 2 h. The mixture was concentrated and the residue was purified by preparative reverse-phase HPLC (solvent A consisting of 10 mM NH<sub>4</sub>-HCO<sub>3</sub>, pH 7.5; solvent B consisting of MeCN) using a linear gradient of 20% B to 100% B over 20 min (see Chemistry: General Methods and Materials for further details) to afford the title compound (3.0 mg, 17%) as a white solid: *t*<sub>R</sub> = 9.6 min; <sup>1</sup>H NMR (600 MHz, CD<sub>3</sub>OD) δ 5.68 (s, 2H), 6.71 (d, *J* = 8.4 Hz, 2H), 7.25 (d, *J* = 8.4 Hz, 2H), 7.49 (t, *J* = 7.2 Hz, 1H), 7.54 (t, *J* = 7.2 Hz, 2H), 8.23 (ovlp d, *J* = 7.2 Hz, 2H), 8.24 (ovlp s, 1H), 8.40 (s, 1H); <sup>13</sup>C NMR (150 MHz, CD<sub>3</sub>OD) δ 51.4, 113.9, 116.2, 116.3, 128.6, 129.4, 130.0, 130.5, 130.8, 134.3, 134.5, 140.1, 152.7, 158.2, 158.6, 165.2; HRMS (ESI-) calcd for C<sub>20</sub>H<sub>14</sub>N<sub>3</sub>O<sub>3</sub> [M - H]<sup>-</sup> 344.1041, found 344.1038 (error 0.9 ppm).

**Ethyl 6-Phenyl-1H-pyrazolo[3,4-b]pyridine-4-carboxylate (112).** A mixture of **111** (340 mg, 0.88 mmol) and TFA (4 mL) was heated at 70 °C for 24 h. Evaporation under vacuum followed by purification of the residue by flash chromatography (7:3 hexanes/EtOAc) afforded the title compound (199 mg, 85%) as a white solid: *R*<sub>f</sub> = 0.51 (3:2 hexanes/EtOAc); <sup>1</sup>H NMR (600 MHz, CDCl<sub>3</sub>) δ 1.53 (t, *J* = 7.2 Hz, 3H), 4.57 (q, *J* = 7.2 Hz, 2H), 7.51 (t, *J* = 7.2 Hz, 1H), 7.56 (t, *J* = 7.2 Hz, 2H), 8.16 (d, *J* = 7.2 Hz, 2H), 8.28 (s, 1H), 8.52 (s, 1H); <sup>13</sup>C NMR (150 MHz, CDCl<sub>3</sub>) δ 14.5, 62.2, 111.8, 116.2, 127.9, 129.2, 130.1, 132.4, 135.1, 138.6, 153.4, 158.0, 165.3; HRMS (ESI+) calcd for C<sub>15</sub>H<sub>14</sub>N<sub>3</sub>O<sub>2</sub> [M + H]<sup>+</sup> 268.1081, found 268.1056 (error 9.3 ppm).

**6-Phenyl-1H-pyrazolo[3,4-b]pyridine-4-carboxylic Acid (36).** To a solution of **112** (30 mg, 0.11 mmol) in THF (1.0 mL) was added 1 N aqueous NaOH (0.6 mL). The resultant solution was stirred at room

temperature for 5 h. The mixture was concentrated and the residue was purified by preparative reverse-phase HPLC (solvent A consisting of 10 mM NH<sub>4</sub>-HCO<sub>3</sub>, pH 7.5; solvent B consisting of MeCN) using a linear gradient of 10% B to 40% B over 20 min (see Chemistry: General Methods and Materials for further details) to afford the title compound (23 mg, 86%) as a white solid: *t*<sub>R</sub> = 18.9 min; <sup>1</sup>H NMR (600 MHz, CD<sub>3</sub>OD) δ 7.45 (t, *J* = 7.2 Hz, 1H), 7.51 (t, *J* = 7.2 Hz, 2H), 8.13 (s, 1H), 8.15 (d, *J* = 7.2 Hz, 2H), 8.47 (s, 1H); <sup>13</sup>C NMR (150 MHz, CD<sub>3</sub>OD) δ 113.8, 115.8, 128.6, 129.8, 130.5, 135.9, 140.7, 142.2, 150.3, 159.9, 172.5; HRMS (ESI-) calcd for C<sub>13</sub>H<sub>8</sub>N<sub>3</sub>O<sub>2</sub> [M - H]<sup>-</sup>, 238.0622; found 238.0617 (error 2.1 ppm).

**1-(4-Methoxybenzyl)-6-(phenylamino)-1H-pyrazolo[3,4-b]pyridine-4-carboxylic Acid (100).** A mixture of **110** (100 mg, 0.22 mmol, 1.0 equiv), Pd(OAc)<sub>2</sub> (5 mg, 0.022 mmol, 0.1 equiv), BINAP (20.4 mg, 0.033 mmol, 0.15 equiv), Cs<sub>2</sub>CO<sub>3</sub> (107 mg, 0.33 mmol, 1.5 equiv), aniline (30 μL, 0.33 mmol, 1.5 equiv), and dioxane (1.5 mL) in a pressure vessel was stirred at 100 °C for 22 h. The reaction mixture was cooled to room temperature, diluted with EtOAc (10 mL), filtered through a plug of Celite, and concentrated. Purification by flash chromatography (4:1 hexanes/EtOAc) afforded ethyl 1-(4-methoxybenzyl)-6-(phenylamino)-1H-pyrazolo[3,4-b]pyridine-4-carboxylate (83 mg, 90%) as a light yellow solid: *R*<sub>f</sub> = 0.53 (3:2 hexanes/EtOAc); <sup>1</sup>H NMR (600 MHz, CDCl<sub>3</sub>) δ 1.45 (t, *J* = 7.2 Hz, 3H), 3.76 (s, 3H), 4.46 (q, *J* = 7.2 Hz, 2H), 5.55 (s, 2H), 6.84 (d, *J* = 8.4 Hz, 2H), 6.87 (br s, 1H, NH), 7.11 (t, *J* = 7.8 Hz, 1H), 7.22 (s, 1H), 7.33 (d, *J* = 8.4 Hz, 2H), 7.38 (t, *J* = 7.8 Hz, 2H), 7.63 (d, *J* = 7.8 Hz, 2H), 8.18 (s, 1H); <sup>13</sup>C NMR (150 MHz, CDCl<sub>3</sub>) δ 14.5, 50.7, 55.5, 62.1, 107.5, 108.6, 114.2, 120.1, 123.4, 129.4, 129.6, 129.7, 133.2, 133.6, 140.1, 150.9, 155.1, 159.4, 165.4.

To a solution of ethyl 1-(4-methoxybenzyl)-6-(phenylamino)-1H-pyrazolo[3,4-b]pyridine-4-carboxylate prepared above (30 mg, 0.074 mmol) in THF (1.0 mL) was added 1 N aqueous NaOH (2 mL). The resulting solution was stirred at room temperature for 3 h. The mixture was concentrated, and H<sub>2</sub>O (10 mL) was added to the residue. The pH was adjusted to 4–5 with 1 N aqueous HCl and the solution extracted with EtOAc (3 × 15 mL). The combined organic layers were dried (MgSO<sub>4</sub>) and concentrated. Purification by flash chromatography (3:7 EtOAc/MeOH) afforded the title compound (19 mg, 69%) as a yellow solid: <sup>1</sup>H NMR (600 MHz, CDCl<sub>3</sub>) δ 3.72 (s, 3H), 5.47 (s, 2H), 6.83 (d, *J* = 9.0 Hz, 2H), 6.97 (t, *J* = 7.8 Hz, 1H), 7.16 (s, 1H), 7.26 (d, *J* = 9.0 Hz, 2H), 7.29 (t, *J* = 7.8 Hz, 2H), 7.79 (d, *J* = 7.8 Hz, 2H), 8.23 (s, 1H); <sup>13</sup>C NMR (150 MHz, CDCl<sub>3</sub>) δ 51.1, 55.7, 108.9, 110.2, 114.9, 120.1, 122.8, 129.7, 130.1, 131.0, 135.0, 141.3, 142.5, 151.9, 157.5, 160.7, 173.2; HRMS (ESI-) calcd for C<sub>21</sub>H<sub>17</sub>N<sub>4</sub>O<sub>3</sub> [M - H]<sup>-</sup> 373.1306, found 373.1282 (error 6.4 ppm).

**Compounds from Scheme 3.** See Supporting Information for the experimental details and data for 37–41, 43–62, and 66–92, which were prepared analogously to 15 and 42, whose experimental details are included below as representative examples.

**General Procedure for Suzuki Coupling of 109.** To a solution of **109** (100 mg, 0.335 mmol, 1.0 equiv) and triethylamine (141 μL, 1.00 mmol, 3.0 equiv) in dioxane (2.5 mL) in an 8 mL heavy-walled screw-cap round-bottom vial was added PyBroP (187 mg, 0.402 mmol, 1.2 equiv). The reaction mixture was shaken on a Glas-Col heater/shaker (Glas-Col LLC, Terre Haute, IN) at room temperature for 2 h. The desired boronic acid (0.67 mmol, 2.0 equiv), PdCl<sub>2</sub>dppf (12 mg, 0.05 equiv), and Na<sub>2</sub>CO<sub>3</sub> (0.7 mL of a 0.254 g/mL aqueous solution, 5.0 equiv) were added. The vial was sealed, and the mixture was heated at 100 °C for 4 h with shaking. The reaction mixture was cooled to room temperature and the solvent removed on a Genevac instrument at 45 °C. The residue was resuspended in H<sub>2</sub>O (2 mL) and extracted with CH<sub>2</sub>Cl<sub>2</sub> (3 mL) using a 6 mL Biotage Isolute phase separator cartridge (Biotage, Charlottesville, VA). The organic layer was concentrated and the residue purified by flash chromatography (hexanes/EtOAc gradient) on a Combiflash Companion system, using a 4 g prepacked silica column, to afford the desired product.

**General Procedure for Ester Hydrolysis.** To a solution of the ester (typically 50 mg, 1 equiv) in THF (1 mL) in an 8 mL vial was added 1 N aqueous NaOH (5.0 mL, 5 equiv). The resulting cloudy solution was stirred at room temperature for 4 h. The solvent was removed

under vacuum at 45 °C on a Genevac instrument. The residue was resuspended in H<sub>2</sub>O (2 mL) and neutralized with 12 N HCl (0.29 mL, 3.5 equiv). Methanol or DMSO were added when necessary to fully dissolve the products, which were purified by preparative reverse-phase HPLC using the indicated methods. Lyophilization of the fractions containing the product afforded the title compounds.

**Ethyl 6-Phenyl-1-(pyridin-4-ylmethyl)-1H-pyrazolo[3,4-b]pyridine-4-carboxylate (18).** The title compound was prepared using the general procedure for Suzuki coupling of **109** (0.40 g, 1.34 mmol, 1.0 equiv) using phenylboronic acid (327 mg, 2.68 mmol, 2.0 equiv). Purification by flash chromatography afforded the title compound (326 mg, 74%) as a white solid:  $R_f$  = 0.39 (EtOAc); <sup>1</sup>H NMR (600 MHz, CDCl<sub>3</sub>) δ 1.52 (t,  $J$  = 7.2 Hz, 3H), 4.55 (q,  $J$  = 7.2 Hz, 2H), 5.82 (s, 2H), 7.22 (d,  $J$  = 6.0 Hz, 2H), 7.49 (t,  $J$  = 7.2 Hz, 1H), 7.53 (t,  $J$  = 7.2 Hz, 2H), 8.17 (d,  $J$  = 7.2 Hz, 2H), 8.29 (s, 1H), 8.46 (s, 1H), 8.55 (d,  $J$  = 6.0 Hz, 2H); <sup>13</sup>C NMR (150 MHz, CDCl<sub>3</sub>) δ 14.5, 49.8, 62.2, 112.1, 115.8, 122.6, 127.6, 129.0, 130.1, 132.4, 134.0, 138.3, 145.8, 150.3, 151.9, 157.4, 165.2; HRMS (ESI<sup>+</sup>) calcd for C<sub>21</sub>H<sub>19</sub>N<sub>4</sub>O<sub>2</sub> [M + H]<sup>+</sup> 359.1503, found 359.1527 (error 6.7 ppm).

**6-Phenyl-1-(pyridin-4-ylmethyl)-1H-pyrazolo[3,4-b]pyridine-4-carboxylic Acid (15).** Compound **18** (120 mg, 0.324 mmol, 1.0 equiv) was converted to the title compound using the general procedure for ester hydrolysis. Purification by preparative reverse-phase HPLC using method 2 followed by lyophilization of the pooled product fractions afforded the title compound (87 mg, 81%) as a white solid:  $t_R$  = 11.0 min; <sup>1</sup>H NMR (600 MHz, CD<sub>3</sub>OD) δ 5.86 (s, 2H), 7.30 (d,  $J$  = 6.0 Hz, 2H), 7.45 (t,  $J$  = 7.2 Hz, 1H), 7.50 (t,  $J$  = 7.2 Hz, 2H), 8.18 (d,  $J$  = 7.2 Hz, 2H), 8.19 (s, 1H), 8.46 (d,  $J$  = 6.0 Hz, 2H), 8.53 (s, 1H); <sup>13</sup>C NMR (150 MHz, CD<sub>3</sub>OD) δ 50.3, 114.7, 116.1, 124.1, 128.6, 129.8, 130.6, 135.9, 140.4, 143.1, 149.3, 150.3, 153.2, 158.9, 172.4; HRMS (ESI<sup>−</sup>) calcd for C<sub>19</sub>H<sub>13</sub>N<sub>4</sub>O<sub>2</sub> [M − H]<sup>−</sup> 329.1044, found 329.1040 (error 1.2 ppm).

**6-(4-Hydroxyphenyl)-1-(pyridin-4-ylmethyl)-1H-pyrazolo[3,4-b]pyridine-4-carboxylic Acid (42).** Ethyl 6-(4-hydroxyphenyl)-1-(pyridin-4-ylmethyl)-1H-pyrazolo[3,4-b]pyridine-4-carboxylate (**42**-ethyl ester) was prepared using the general procedure for Suzuki coupling of **109** with 4-hydroxyphenylboronic acid (92 mg, 0.67 mmol, 2 equiv). Purification by flash chromatography afforded **42**-ethyl ester (78 mg, 62%) as a white solid:  $R_f$  = 0.22 (EtOAc); <sup>1</sup>H NMR (600 MHz, DMSO-*d*<sub>6</sub>) δ 1.44 (t,  $J$  = 7.2 Hz, 3H), 4.49 (q,  $J$  = 7.2 Hz, 2H), 5.83 (s, 2H), 6.92 (d,  $J$  = 8.4 Hz, 2H), 7.19 (d,  $J$  = 5.4 Hz, 2H), 8.10 (d,  $J$  = 8.4 Hz, 2H), 8.16 (s, 1H), 8.41 (s, 1H), 8.50 (d,  $J$  = 5.4 Hz, 2H), 9.98 (s, 1H, OH); <sup>13</sup>C NMR (150 MHz, DMSO-*d*<sub>6</sub>) δ 14.1, 48.9, 61.8, 110.6, 114.1, 115.9, 122.2, 128.3, 129.0, 131.9, 133.2, 146.1, 149.9, 151.4, 156.4, 159.6, 164.6.

The **42**-ethyl ester (50 mg, 0.133 mmol, 1.0 equiv) prepared above was converted to the title compound using the general procedure for ester hydrolysis. Purification by preparative reverse-phase HPLC using method 2 afforded the title compound (43 mg, 93%) as a white solid:  $t_R$  = 8.0 min; <sup>1</sup>H NMR (600 MHz, CD<sub>3</sub>OD) δ 5.83 (s, 2H), 6.89 (d,  $J$  = 8.4 Hz, 2H), 7.29 (d,  $J$  = 5.4 Hz, 2H), 8.05 (d,  $J$  = 8.4 Hz, 2H), 8.11 (s, 1H), 8.46 (d,  $J$  = 5.4 Hz, 2H), 8.48 (s, 1H); <sup>13</sup>C NMR (150 MHz, CD<sub>3</sub>OD) δ 50.2, 113.9, 115.5, 116.7, 124.1, 130.1, 131.5, 142.8, 149.4, 150.3, 153.2, 159.1, 159.4, 160.8, 172.6; HRMS (ESI<sup>−</sup>) calcd for C<sub>19</sub>H<sub>13</sub>N<sub>4</sub>O<sub>3</sub> [M − H]<sup>−</sup> 345.0993, found 345.0999 (error 1.7 ppm).

**General Procedure for Amination of 109.** To a solution of **109** (100 mg, 0.335 mmol, 1.0 equiv) and BOP (193 mg, 0.437 mmol, 1.3 equiv) in dioxane (3 mL) in an 8 mL vial was added DBU (76 μL, 0.504 mmol, 1.5 equiv), and the resulting mixture was stirred for 15 min at room temperature. The desired amine (1.01 mmol, 3 equiv) was added. The vial was sealed, and the reaction mixture was heated at 70 °C with stirring for 5 h. The reaction mixture was concentrated. Then the residue was resuspended in H<sub>2</sub>O (10 mL) and extracted with EtOAc (3 × 15 mL). The combined organic layers were dried (MgSO<sub>4</sub>) and concentrated. Purification by flash chromatography (hexane/EtOAc gradient) on a Combiflash Companion system, using a 4 g prepacked silica column, afforded the desired product.

**6-(Benzylamino)-1-(pyridin-4-ylmethyl)-1H-pyrazolo[3,4-b]pyridine-4-carboxylic Acid (95).** Ethyl 6-(benzylamino)-1-(pyridin-4-ylmethyl)-1H-pyrazolo[3,4-b]pyridine-4-carboxylate was prepared

using the general procedure for amination of **109** with benzylamine (110 μL, 1.01 mmol, 3 equiv). Purification by flash chromatography afforded the ethyl ester of the title compound (28 mg, 22%) as a white solid:  $R_f$  = 0.42 (EtOAc); <sup>1</sup>H NMR (600 MHz, CDCl<sub>3</sub>) δ 1.44 (t,  $J$  = 7.2 Hz, 3H), 4.43 (q,  $J$  = 7.2 Hz, 2H), 4.66 (d,  $J$  = 6.0 Hz, 2H), 5.50 (ovlp t,  $J$  = 6.0 Hz, 1H, NH), 5.52 (ovlp s, 2H), 7.02 (s, 1H), 7.07 (d,  $J$  = 5.4 Hz, 2H), 7.26 (t,  $J$  = 7.2 Hz, 1H), 7.29 (t,  $J$  = 7.2 Hz, 2H), 7.33 (d,  $J$  = 7.2 Hz, 2H), 8.15 (s, 1H), 8.46 (d,  $J$  = 5.4 Hz, 2H); <sup>13</sup>C NMR (150 MHz, CDCl<sub>3</sub>) δ 14.4, 45.9, 49.4, 61.9, 105.1, 108.3, 122.7, 127.5, 127.7, 128.8, 132.9, 134.2, 139.0, 146.3, 150.0, 151.7, 158.0, 165.4.

Ethyl 6-(benzylamino)-1-(pyridin-4-ylmethyl)-1H-pyrazolo[3,4-b]pyridine-4-carboxylate prepared above (20 mg, 0.052 mmol, 1.0 equiv) was converted to the title compound using the general procedure for ester hydrolysis. Purification by preparative reverse-phase HPLC using method 4 afforded the title compound as a white solid (17 mg, 91%):  $t_R$  = 10.0 min; <sup>1</sup>H NMR (600 MHz, CD<sub>3</sub>OD) δ 4.60 (s, 2H), 5.51 (s, 2H), 6.92 (s, 1H), 7.10 (d,  $J$  = 6.0 Hz, 2H), 7.17 (t,  $J$  = 7.2 Hz, 1H), 7.21 (t,  $J$  = 7.2 Hz, 2H), 7.31 (d,  $J$  = 7.2 Hz, 2H), 8.13 (s, 1H), 8.34 (d,  $J$  = 6.0 Hz, 2H); <sup>13</sup>C NMR (150 MHz, DMSO-*d*<sub>6</sub>) δ 44.2, 48.5, 104.9, 122.3, 122.5, 127.4, 127.7, 128.0, 128.3, 139.8, 146.4, 149.6, 149.8, 151.2, 158.3, 166.3; HRMS (ESI<sup>−</sup>) calcd for C<sub>20</sub>H<sub>16</sub>N<sub>5</sub>O<sub>2</sub> [M − H]<sup>−</sup> 358.1309, found 358.1316 (error 2.0 ppm).

**6-Morpholino-1-(pyridin-4-ylmethyl)-1H-pyrazolo[3,4-b]pyridine-4-carboxylic Acid (96).** Ethyl 6-morpholino-1-(pyridin-4-ylmethyl)-1H-pyrazolo[3,4-b]pyridine-4-carboxylate was prepared using the general procedure for amination of **109** with morpholine (88 μL, 1.01 mmol, 3 equiv). Purification by flash chromatography afforded the ethyl ester of the title compound (98 mg, 79%) as a pale yellow solid:  $R_f$  = 0.37 (EtOAc); <sup>1</sup>H NMR (600 MHz, CDCl<sub>3</sub>) δ 1.48 (t,  $J$  = 7.2 Hz, 3H), 3.68 (t,  $J$  = 4.8 Hz, 4H), 3.83 (t,  $J$  = 4.8 Hz, 4H), 4.49 (q,  $J$  = 7.2 Hz, 2H), 5.56 (s, 2H), 7.12 (d,  $J$  = 6.0 Hz, 2H), 7.27 (s, 1H), 8.18 (s, 1H), 8.52 (d,  $J$  = 6.0 Hz, 2H); <sup>13</sup>C NMR (150 MHz, CDCl<sub>3</sub>) δ 14.5, 45.8, 49.4, 62.1, 66.8, 105.5, 106.3, 122.6, 133.3, 134.2, 146.4, 150.1, 151.5, 158.9, 165.6.

Ethyl 6-morpholino-1-(pyridin-4-ylmethyl)-1H-pyrazolo[3,4-b]pyridine-4-carboxylate prepared above (98 mg, 0.267 mmol, 1.0 equiv) was converted to the title compound using the general procedure for ester hydrolysis. Purification by preparative reverse-phase HPLC using method 4 afforded the title compound (45 mg, 97%) as a pale yellow solid:  $t_R$  = 6.5 min; <sup>1</sup>H NMR (600 MHz, DMSO-*d*<sub>6</sub>) δ 3.62 (t,  $J$  = 4.8 Hz, 4H), 3.70 (t,  $J$  = 4.8 Hz, 4H), 5.56 (s, 2H), 7.14 (d,  $J$  = 6.0 Hz, 2H), 7.26 (s, 1H), 8.10 (s, 1H), 8.48 (d,  $J$  = 6.0 Hz, 2H); <sup>13</sup>C NMR (150 MHz, CD<sub>3</sub>OD) δ 45.2, 48.6, 65.9, 105.1, 105.7, 122.4, 133.2, 133.9, 146.4, 149.8, 150.9, 158.6, 166.3; HRMS (ESI<sup>−</sup>) calcd for C<sub>17</sub>H<sub>16</sub>N<sub>5</sub>O<sub>3</sub> [M − H]<sup>−</sup> 338.1259, found 338.1262 (error 0.9 ppm).

**6-(3-Hydroxypropylamino)-1-(pyridin-4-ylmethyl)-1H-pyrazolo[3,4-b]pyridine-4-carboxylic Acid (97).** Ethyl 6-(3-hydroxypropylamino)-1-(pyridin-4-ylmethyl)-1H-pyrazolo[3,4-b]pyridine-4-carboxylate was prepared using the general procedure for amination of **109** with 3-hydroxypropylamine (77 μL, 1.01 mmol, 3 equiv). The crude product obtained after extraction was converted to the title compound using the general procedure for ester hydrolysis. Purification by preparative reverse-phase HPLC using method 4 afforded the title compound (22 mg, 18% over two steps) as a white solid:  $t_R$  = 8.6 min; <sup>1</sup>H NMR (600 MHz, DMSO-*d*<sub>6</sub>) δ 1.70 (pent,  $J$  = 6.6 Hz, 2H), 3.37 (t,  $J$  = 6.6 Hz, 2H), 3.48 (t,  $J$  = 6.6 Hz, 2H), 5.50 (s, 2H), 7.01 (s, 1H), 7.15 (d,  $J$  = 4.8 Hz, 2H), 7.98 (s, 1H), 8.47 (d,  $J$  = 4.8 Hz, 2H); <sup>13</sup>C NMR (150 MHz, DMSO-*d*<sub>6</sub>) δ 31.9, 38.0, 48.7, 58.7, 99.5, 104.6, 122.6, 132.5, 133.3, 146.8, 149.8, 151.8, 158.8, 166.4; HRMS (ESI<sup>−</sup>) calcd for C<sub>16</sub>H<sub>16</sub>N<sub>5</sub>O<sub>3</sub> [M − H]<sup>−</sup> 326.1259, found 326.1260 (error 0.3 ppm).

**6-Oxo-1-(pyridin-4-ylmethyl)-6,7-dihydro-1H-pyrazolo[3,4-b]pyridine-4-carboxylic Acid (98).** Compound **109** (40 mg, 0.134 mmol, 1.0 equiv) was converted to the title compound using the general procedure for ester hydrolysis. Purification by preparative HPLC using method 5 afforded the title compound (26 mg, 72%) as a white solid:  $t_R$  = 8.0 min; <sup>1</sup>H NMR (600 MHz, CD<sub>3</sub>OD) δ 5.59 (s, 2H), 6.86 (s, 1H), 7.17 (d,  $J$  = 6.0 Hz, 2H), 8.21 (s, 1H), 8.44 (d,  $J$  = 6.0 Hz, 2H); <sup>13</sup>C NMR (150 MHz, CD<sub>3</sub>OD) δ 50.0, 108.4, 111.5, 123.8, 136.4, 144.9, 149.5, 150.2, 150.9, 169.5, 172.8; HRMS (ESI<sup>−</sup>)



calcd for  $C_{13}H_9N_4O_3$   $[M - H]^-$  269.0680, found 269.0682 (error 0.7 ppm).

**Compounds from Scheme 4.** See Supporting Information for the experimental details and data for **60** and **64–65**, which were prepared analogously to **43**, whose experimentals are included below as a representative example.

**General Procedure for Alkylation of 42-Ethyl Ester and Hydrolysis.** To a solution of 42-ethyl ester (112.3 mg, 0.30 mmol, 1.0 equiv) and  $Na_2CO_3$  (63.6 mg, 0.6 mmol, 2.0 equiv) in 1:1 dioxane– $H_2O$  (6 mL) was added the respective alkyl bromide (1.2 mmol, 4.0 equiv). The mixture was heated at 80 °C for 12 h and then cooled to room temperature, and the crude mixture was extracted with EtOAc (3 × 15 mL). The combined organic layers were washed with saturated aqueous NaCl (20 mL), dried ( $MgSO_4$ ), and concentrated. The crude residue was purified by flash chromatography (4:1 EtOAc–hexane) to afford the ethyl esters of the title compounds. Hydrolysis of the ethyl esters was accomplished by dissolving the intermediate ethyl esters (0.30 mmol, 1.0 equiv) in THF (3 mL) followed by the addition of 1 N aqueous NaOH (3 mL, 3 mmol, 10 equiv). The resulting solution was stirred at 60 °C for 12 h and then cooled to room temperature. The pH was adjusted to ~6 by the addition of 1 N aqueous HCl, and the crude mixture was extracted with 10:1 EtOAc–MeOH (5 × 15 mL). The combined organic extracts were washed with saturated aqueous NaCl (20 mL), dried ( $MgSO_4$ ), and concentrated. The products were dissolved in EtOAc with a small amount of MeOH to aid in dissolution and then triturated with hexane, whereupon the products precipitated as analytically pure white solids in yields ranging from 40% to 70%.

**6-[4-(Octyloxy)phenyl]-1-(pyridin-4-ylmethyl)-1H-pyrazolo[3,4-b]pyridine-4-carboxylic Acid (63).** The title compound was prepared using the general procedure for alkylation of 42-ethyl ester and hydrolysis employing octyl bromide (210  $\mu$ L, 1.2 mmol) to afford the title compound (38 mg, 28% over two steps) as a white solid:  $R_f$  = 0.22 (1:4 MeOH/EtOAc);  $^1H$  NMR (600 MHz,  $DMSO-d_6$ )  $\delta$  0.86 (t,  $J$  = 7.2 Hz, 3H), 1.27–1.32 (m, 8H), 1.41–1.42 (m, 2H), 1.72–1.75 (m, 2H), 4.04 (t,  $J$  = 7.2 Hz, 2H), 5.84 (s, 2H), 7.07 (d,  $J$  = 8.2 Hz, 2H), 7.20 (d,  $J$  = 3.2 Hz, 2H), 8.17–8.19 (m, 3H), 8.41 (s, 1H), 8.50 (d,  $J$  = 3.2 Hz, 2H);  $^{13}C$  NMR (150 MHz,  $DMSO-d_6$ )  $\delta$  14.0, 22.1, 25.5, 28.62, 28.65, 28.7, 31.2, 48.9, 67.6, 111.6, 114.3, 114.8, 122.3, 128.8, 130.0, 133.5, 141.5, 146.2, 149.9, 151.4, 156.0, 160.3, 170.4; HRMS (ESI $^-$ ) calcd for  $C_{27}H_{29}N_4O_3$   $[M - H]^-$  457.2245, found 457.2220 (error 5.5 ppm).

**6-Ethynyl-1-(pyridin-4-ylmethyl)-1H-pyrazolo[3,4-b]pyridine-4-carboxylic Acid (93).** A 1.0 M solution of TBAF in THF (0.25 mL, 1.0 equiv) was added to a solution of **114**<sup>45</sup> (105 mg, 0.25 mmol, 1.0 equiv) in THF (10 mL) at 0 °C and stirred for 3 h. The reaction mixture was diluted with  $H_2O$  (10 mL) and extracted with  $CH_2Cl_2$  (3 × 15 mL). The combined organic layers were dried ( $MgSO_4$ ) and concentrated. Purification by flash chromatography (hexane–EtOAc gradient) afforded **116** (27 mg, 35%) as a white solid:  $R_f$  = 0.54 (EtOAc);  $^1H$  NMR (600 MHz,  $CDCl_3$ )  $\delta$  1.48 (t,  $J$  = 7.2 Hz, 3H), 3.32 (s, 1H), 4.52 (q,  $J$  = 7.2 Hz, 2H), 5.75 (s, 2H), 7.13 (d,  $J$  = 4.8 Hz, 2H), 7.94 (s, 1H), 8.48 (s, 1H), 8.53 (d,  $J$  = 4.8 Hz, 2H);  $^{13}C$  NMR (150 MHz,  $CDCl_3$ )  $\delta$  14.4, 49.8, 62.4, 72.3, 82.7, 113.0, 122.0, 122.6, 132.1, 134.1, 141.5, 145.4, 150.3, 151.3, 164.4.

Compound **116** prepared above (20 mg, 0.065 mmol, 1.0 equiv) was converted to the title compound using the general procedure for ester hydrolysis. Purification by preparative reverse-phase HPLC using method 4 afforded the title compound (7.4 mg, 41%) as an off-white solid:  $t_R$  = 8.3 min;  $^1H$  NMR (400 MHz,  $DMSO-d_6$ )  $\delta$  4.64 (s, 1H), 5.78 (s, 2H), 7.12 (d,  $J$  = 6.0 Hz, 2H), 7.74 (s, 1H), 8.50 (d,  $J$  = 6.0 Hz, 2H), 8.51 (s, 1H);  $^{13}C$  NMR (100 MHz,  $DMSO-d_6$ )  $\delta$  49.0, 82.4, 82.8, 99.5, 112.9, 121.0, 122.0, 133.7, 140.7, 145.9, 149.9, 150.8, 165.3; HRMS (ESI $^-$ ) calcd for  $C_{15}H_9N_4O_2$   $[M - H]^-$  277.0731, found 277.0736 (error 1.8 ppm).

**6-(Phenylethynyl)-1-(pyridin-4-ylmethyl)-1H-pyrazolo[3,4-b]pyridine-4-carboxylic Acid (94).** Compound **115**<sup>45</sup> (60 mg, 0.157 mmol, 1.0 equiv) was converted to the title compound using the general procedure for ester hydrolysis. Purification by preparative reverse-phase HPLC using method 2 afforded the title compound (36

mg, 65%) as a white solid:  $t_R$  = 11.8 min;  $^1H$  NMR (600 MHz,  $DMSO-d_6$ )  $\delta$  5.77 (s, 2H), 7.10 (d,  $J$  = 5.4 Hz, 2H), 7.45–7.50 (m, 3H), 7.68 (dd,  $J$  = 7.8, 2.4 Hz, 2H), 7.77 (s, 1H), 8.49 (d,  $J$  = 5.4 Hz, 2H), 8.54 (s, 1H);  $^{13}C$  NMR (150 MHz,  $DMSO-d_6$ )  $\delta$  48.9, 89.5, 89.6, 113.7, 121.1, 121.2, 121.9, 128.9, 129.7, 131.9, 134.7, 141.1, 146.4, 149.8, 151.1, 165.8 (missing one aryl carbon); HRMS (ESI $^-$ ) calcd for  $C_{21}H_{13}N_4O_2$   $[M - H]^-$  353.1044, found 353.1035 (error 2.5 ppm).

**Compounds from Scheme 5.** See Supporting Information for the experimental details and data for **23–25**, **27**, and **28**, which were prepared analogously to **22**, whose experimental details are included below as a representative example.

**4-Hydroxymethyl-6-phenyl-1-(pyridin-4-ylmethyl)-1H-pyrazolo[3,4-b]pyridine (19).** A solution of **18** (358 mg, 1.0 mmol, 1.0 equiv) in THF (2 mL) was slowly added to a suspension of  $LiAlH_4$  (57 mg, 1.5 mmol, 1.5 equiv) in THF (8.0 mL) at 0 °C. The reaction mixture was stirred at 0 °C for 10 min and gradually warmed to 22 °C over 1 h. After the mixture was stirred for 2 h at 22 °C, the reaction was quenched with MeOH (5 mL) and the mixture diluted with  $CH_2Cl_2$  (15 mL). The organic layer was washed consecutively with saturated aqueous  $NH_4Cl$  (10 mL),  $H_2O$  (10 mL), saturated aqueous NaCl (10 mL), then dried ( $Na_2SO_4$ ) and concentrated. Purification by flash chromatography (10:1 to 5:1  $CH_2Cl_2$ –MeOH) afforded the title compound **19** (143 mg, 45%) as a white solid:  $R_f$  = 0.36 (EtOAc);  $^1H$  NMR (600 MHz,  $CDCl_3$ )  $\delta$  5.09 (s, 2H), 5.75 (s, 2H), 7.15 (d,  $J$  = 6.0 Hz, 2H), 7.43 (t,  $J$  = 7.2 Hz, 1H), 7.47 (t,  $J$  = 7.2 Hz, 2H), 7.65 (s, 1H), 8.08 (d,  $J$  = 7.2 Hz, 2H), 8.16 (s, 1H), 8.42 (d,  $J$  = 6.0 Hz, 2H);  $^{13}C$  NMR (150 MHz,  $CDCl_3$ )  $\delta$  49.5, 62.7, 111.7, 112.6, 122.8, 127.6, 128.9, 129.7, 132.3, 139.2, 146.2, 146.6, 149.8, 151.3, 157.4; HRMS (ESI $^+$ ) calcd for  $C_{19}H_{17}N_4O$   $[M]^+$  317.1397, found 317.1395 (error 0.6 ppm).

**6-Phenyl-1-(pyridin-4-ylmethyl)-1H-pyrazolo[3,4-b]pyridine-4-amine (21).** Compound **15** (50 mg, 0.168 mmol, 1.0 equiv) was dissolved in 3:1  $CH_2Cl_2$ –THF (4 mL), and oxalyl chloride (17.6  $\mu$ L, 0.205 mmol, 1.2 equiv) was slowly added at room temperature. The reaction mixture was stirred for 4 h and then concentrated in vacuo. The residue was dissolved in acetone (5 mL) and added to a solution of  $NaN_3$  (47 mg, 0.73 mmol, 4.3 equiv) in  $H_2O$  (5 mL). The solution was immediately extracted with EtOAc (2 × 20 mL). The combined organic layers were dried ( $MgSO_4$ ), and the solvent was removed under vacuum. The residue was dissolved in benzene (5 mL). Then TFA (19  $\mu$ L, 0.25 mmol, 1.5 equiv) was added, and the solution was refluxed for 16 h. The solution was concentrated and the residue redissolved in MeOH (5 mL). Solid  $K_2CO_3$  (51 mg, 0.37 mmol, 2.2 equiv) was added, and the reaction mixture was stirred vigorously for 8 h at room temperature. The mixture was concentrated and the residue partitioned between  $H_2O$  (10 mL) and EtOAc (3 × 15 mL). The combined organic layers were dried ( $MgSO_4$ ), and the solvent was removed under vacuum. Purification by flash chromatography (hexanes/EtOAc gradient) afforded the title compound (16 mg, 31%) as a white solid:  $R_f$  = 0.36 (EtOAc);  $^1H$  NMR (600 MHz,  $CDCl_3$ )  $\delta$  4.80 (br s, 2H,  $NH_2$ ), 5.70 (s, 2H), 6.78 (s, 1H), 7.21 (d,  $J$  = 4.8 Hz, 2H), 7.41 (t,  $J$  = 7.2 Hz, 1H), 7.46 (t,  $J$  = 7.2 Hz, 2H), 7.97 (s, 1H), 8.02 (d,  $J$  = 7.2 Hz, 2H), 8.54 (br s, 2H);  $^{13}C$  NMR (150 MHz,  $CDCl_3$ )  $\delta$  49.6, 98.5, 104.7, 122.8, 127.5, 128.7, 129.3, 130.2, 139.9, 146.5, 148.2, 150.1, 152.9, 158.6; HRMS (ESI $^-$ ) calcd for  $C_{18}H_{14}N_5O$   $[M - H]^-$  300.1255, found 300.1255 (error 0 ppm).

**General Procedure for the Synthesis of 6-Phenyl-1-(pyridin-4-ylmethyl)-1H-pyrazolo[3,4-b]pyridine-4-carboxamide Analogues.** To a solution of **15** (15 mg, 0.045 mmol, 1.0 equiv) and DMF (3.5  $\mu$ L, 0.045 mmol, 1.0 equiv) in dry  $CH_2Cl_2$  (2 mL) at 0 °C was added oxalyl chloride (7.7  $\mu$ L, 0.090 mmol, 2.0 equiv). The mixture was stirred for 1 h, then concentrated in vacuo. A solution of the desired amine (2–10 equiv) and DMAP (1.8 mg, 0.015 mmol, 0.3 equiv) in  $CH_2Cl_2$  (2.0 mL) was added, and the mixture was stirred for 1 h at room temperature. The mixture was concentrated and the residue resuspended in  $H_2O$  (2 mL). Methanol or DMSO was added if necessary to fully dissolve the products. Purification by preparative HPLC using method 2 followed by lyophilization of the pooled product fractions afforded the title compounds.

**6-Phenyl-1-(pyridin-4-ylmethyl)-1H-pyrazolo[3,4-b]pyridine-4-carboxamide (22).** The title compound was prepared using the general procedure for the synthesis of 4-carboxamide analogues from **15**, using a 14.8 M ammonium hydroxide solution (34  $\mu$ L, 0.50 mmol, 10 equiv). Purification by preparative reverse-phase HPLC using method 2 afforded the title compound (4.9 mg, 30%) as a white solid:  $t_R$  = 12.2 min;  $^1\text{H}$  NMR (600 MHz,  $\text{CD}_3\text{OD}$ )  $\delta$  5.88 (s, 2H), 7.32 (d,  $J$  = 5.4 Hz, 2H), 7.48 (t,  $J$  = 7.2 Hz, 1H), 7.52 (t,  $J$  = 7.2 Hz, 2H), 8.17 (s, 1H), 8.23 (d,  $J$  = 7.2 Hz, 2H), 8.45 (s, 1H), 8.47 (d,  $J$  = 5.4 Hz, 2H);  $^{13}\text{C}$  NMR (150 MHz,  $\text{CD}_3\text{OD}$ )  $\delta$  50.4, 113.2, 114.3, 124.1, 128.7, 130.0, 131.1, 134.7, 138.3, 139.7, 149.0, 150.4, 153.0, 159.1, 169.9; HRMS (ESI+) calcd for  $\text{C}_{19}\text{H}_{16}\text{N}_5\text{O}$  [ $\text{M} + \text{H}$ ] $^+$  330.1349, found 330.1353 (error 1.2 ppm).

**Compounds from Scheme 6. Methyl 6-Bromo-1-(pyridin-4-ylmethyl)-1H-indazole-4-carboxylate (119) and Methyl 6-Bromo-2-(pyridin-4-ylmethyl)-2H-indazole-4-carboxylate (121).** To a solution of methyl 6-bromo-1H-indazole-4-carboxylate **117** (300 mg, 1.18 mmol, 1.0 equiv) in DMF (10 mL) was added  $\text{Cs}_2\text{CO}_3$  (2.3 g, 7.1 mmol, 6.0 equiv), and the resulting suspension was stirred at room temperature for 30 min. 4-(Bromomethyl)pyridine hydrobromide (0.89 g, 3.53 mmol, 3.0 equiv) was added, and stirring continued at room temperature for 3 h. The reaction mixture was diluted with EtOAc (20 mL), filtered through a bed of Celite, and concentrated. Purification by flash chromatography (hexanes/EtOAc gradient) afforded the two title compounds as white solids.

Data for **119** (128 mg, 31%):  $R_f$  = 0.37 (EtOAc);  $^1\text{H}$  NMR (600 MHz,  $\text{CDCl}_3$ )  $\delta$  4.01 (s, 3H), 5.58 (s, 2H), 6.98 (d,  $J$  = 6.0 Hz, 2H), 7.65 (s, 1H), 8.01 (s, 1H), 8.52–8.54 (m, 3H);  $^{13}\text{C}$  NMR (150 MHz,  $\text{CDCl}_3$ )  $\delta$  51.9, 52.7, 116.3, 120.4, 121.7, 122.0, 124.4, 127.9, 135.3, 140.9, 145.1, 150.5, 165.4; HRMS (ESI+) calcd for  $\text{C}_{15}\text{H}_{13}\text{BrN}_3\text{O}_2$  [ $\text{M} + \text{H}$ ] $^+$  348.0186, found 348.0176 (error 2.8 ppm).

Data for **121** (76 mg, 19%):  $R_f$  = 0.19 (EtOAc);  $^1\text{H}$  NMR (600 MHz,  $\text{CDCl}_3$ )  $\delta$  3.95 (s, 3H), 5.60 (s, 2H), 7.07 (d,  $J$  = 6.0 Hz, 2H), 7.97 (s, 1H), 8.09 (s, 1H), 8.47 (s, 1H), 8.57 (d,  $J$  = 6.0 Hz, 2H);  $^{13}\text{C}$  NMR (150 MHz,  $\text{CDCl}_3$ )  $\delta$  52.5, 56.5, 119.2, 119.3, 122.1, 123.9, 125.5, 126.0, 130.0, 144.3, 150.1, 150.6, 165.5; HRMS (ESI+) calcd for  $\text{C}_{15}\text{H}_{13}\text{BrN}_3\text{O}_2$  [ $\text{M} + \text{H}$ ] $^+$  348.0186, found 348.0175 (error 3.2 ppm).

**6-Phenyl-1-(pyridin-4-ylmethyl)-1H-indazole-4-carboxylic Acid (16).** Methyl 6-phenyl-1-(pyridin-4-ylmethyl)-1H-indazole-4-carboxylate was prepared using the general procedure for Suzuki coupling from **119** (50 mg, 0.144 mmol, 1.0 equiv). Purification by flash chromatography (hexanes/EtOAc gradient) afforded the methyl ester of the title compound (28 mg, 57%) as a white solid:  $R_f$  = 0.40 (EtOAc);  $^1\text{H}$  NMR (600 MHz,  $\text{CDCl}_3$ )  $\delta$  4.06 (s, 3H), 5.69 (s, 2H), 7.03 (d,  $J$  = 6.0 Hz, 2H), 7.40 (t,  $J$  = 7.2 Hz, 1H), 7.47 (t,  $J$  = 7.2 Hz, 2H), 7.61 (d,  $J$  = 7.2 Hz, 2H), 7.63 (s, 1H), 8.22 (s, 1H), 8.54 (d,  $J$  = 6.0 Hz, 2H), 8.60 (s, 1H);  $^{13}\text{C}$  NMR (150 MHz,  $\text{CDCl}_3$ )  $\delta$  51.9, 52.5, 111.6, 121.7, 122.2, 123.7, 125.0, 127.7, 128.2, 129.2, 135.1, 140.1, 140.3, 141.0, 145.6, 150.5, 166.6.

Methyl 6-phenyl-1-(pyridin-4-ylmethyl)-1H-indazole-4-carboxylate (23 mg, 0.067 mmol, 1.0 equiv) prepared above was converted to the title compound using the general procedure for ester hydrolysis. Purification by preparative reverse-phase HPLC using method 3 afforded the title compound (16 mg, 72%) as a white solid:  $t_R$  = 9.5 min;  $^1\text{H}$  NMR (400 MHz,  $\text{DMSO}-d_6$ )  $\delta$  5.87 (s, 2H), 7.13 (d,  $J$  = 6.0 Hz, 2H), 7.42 (t,  $J$  = 7.2 Hz, 1H), 7.51 (t,  $J$  = 7.2 Hz, 2H), 7.78 (d,  $J$  = 7.2 Hz, 2H), 8.08 (s, 1H), 8.29 (s, 1H), 8.48–8.50 (m, 3H);  $^{13}\text{C}$  NMR (100 MHz,  $\text{DMSO}-d_6$ )  $\delta$  50.6, 111.4, 121.6, 122.0 (2 C), 123.1, 127.3, 127.9, 129.0, 134.4, 138.4, 139.5, 141.1, 146.4, 149.9, 167.2; HRMS (ESI–) calcd for  $\text{C}_{20}\text{H}_{14}\text{N}_3\text{O}_2$  [ $\text{M} - \text{H}$ ] $^-$  328.1092, found 328.1089 (error 0.9 ppm).

**6-Phenyl-2-(pyridin-4-ylmethyl)-2H-indazole-4-carboxylic Acid (99).** Methyl 6-phenyl-2-(pyridin-4-ylmethyl)-2H-indazole-4-carboxylate was prepared using the general procedure for Suzuki coupling from **121** (50 mg, 0.144 mmol, 1.0 equiv). Purification by flash chromatography (hexanes/EtOAc gradient) afforded the methyl ester of the title compound (38 mg, 77%) as a white solid:  $R_f$  = 0.22 (EtOAc);  $^1\text{H}$  NMR (600 MHz,  $\text{CDCl}_3$ )  $\delta$  3.99 (s, 3H), 5.65 (s, 2H), 7.12 (d,  $J$  = 6.0 Hz, 2H), 7.39 (t,  $J$  = 7.2 Hz, 1H), 7.48 (t,  $J$  = 7.2 Hz, 2H), 7.69 (d,  $J$  = 7.2 Hz, 2H), 8.13 (s, 1H), 8.24 (s, 1H), 8.51 (s, 1H),

8.59 (d,  $J$  = 6.0 Hz, 2H);  $^{13}\text{C}$  NMR (150 MHz,  $\text{CDCl}_3$ )  $\delta$  52.3, 56.5, 119.8, 120.8, 122.1, 122.9, 125.6, 127.4, 127.5, 127.9, 129.1, 139.1, 140.1, 144.7, 150.3, 150.5, 166.6.

Methyl 6-phenyl-2-(pyridin-4-ylmethyl)-2H-indazole-4-carboxylate (34 mg, 0.099 mmol, 1.0 equiv) prepared above was converted to the title compound using the general procedure for ester hydrolysis. Purification by preparative reverse-phase HPLC using method 3 afforded the title compound (25 mg, 77%) as a white solid:  $t_R$  = 9.0 min;  $^1\text{H}$  NMR (400 MHz,  $\text{DMSO}-d_6$ )  $\delta$  5.82 (s, 2H), 7.24 (d,  $J$  = 6.0 Hz, 2H), 7.40 (t,  $J$  = 7.2 Hz, 1H), 7.50 (t,  $J$  = 7.2 Hz, 2H), 7.77 (d,  $J$  = 7.2 Hz, 2H), 8.08 (s, 1H), 8.15 (s, 1H), 8.54 (d,  $J$  = 6.0 Hz, 2H), 8.87 (s, 1H);  $^{13}\text{C}$  NMR (100 MHz,  $\text{DMSO}-d_6$ )  $\delta$  55.1, 119.0, 119.6, 122.5, 124.3, 125.3, 126.3, 127.0, 127.7, 129.1, 137.4, 139.8, 145.6, 149.6, 149.9, 167.0; HRMS (ESI–) calcd for  $\text{C}_{20}\text{H}_{14}\text{N}_3\text{O}_2$  [ $\text{M} - \text{H}$ ] $^-$  328.1092, found 328.1084 (error 2.4 ppm).

**Methyl 6-Bromo-1-(pyridin-4-ylmethyl)-1H-indole-4-carboxylate (120).** To a solution of methyl 6-bromo-1H-indole-4-carboxylate **118** (50 mg, 0.20 mmol, 1.0 equiv) in DMF (3 mL) was added  $\text{Cs}_2\text{CO}_3$  (391 mg, 1.2 mmol, 6.0 equiv), and the resulting suspension was stirred at room temperature for 30 min. 4-(Bromomethyl)pyridine hydrobromide (152 mg, 0.6 mmol, 3.0 equiv) was added, and stirring continued at room temperature for 2 h. The reaction mixture was diluted with EtOAc (10 mL), filtered through a bed of Celite, and concentrated. Purification by flash chromatography (hexanes/EtOAc gradient) afforded the title compound (53 mg, 77%) as a white solid:  $R_f$  = 0.30 (EtOAc);  $^1\text{H}$  NMR (600 MHz,  $\text{CDCl}_3$ )  $\delta$  3.98 (s, 3H), 5.32 (s, 2H), 6.89 (d,  $J$  = 5.4 Hz, 2H), 7.20 (d,  $J$  = 3.0 Hz, 1H), 7.23 (d,  $J$  = 3.0 Hz, 1H), 7.50 (s, 1H), 8.01 (s, 1H), 8.53 (d,  $J$  = 5.4 Hz, 2H);  $^{13}\text{C}$  NMR (150 MHz,  $\text{CDCl}_3$ )  $\delta$  49.3, 52.2, 104.1, 114.8, 116.9, 121.2, 123.3, 125.5, 127.4, 131.1, 137.8, 145.7, 150.6, 166.7; HRMS (ESI+) calcd for  $\text{C}_{16}\text{H}_{14}\text{BrN}_2\text{O}_2$  [ $\text{M} + \text{H}$ ] $^+$  347.0213, found 347.0222 (error 2.6 ppm).

**6-Phenyl-1-(pyridin-4-ylmethyl)-1H-indole-4-carboxylic Acid (17).** Methyl 6-phenyl-1-(pyridin-4-ylmethyl)-1H-indole-4-carboxylate was prepared using the general procedure for Suzuki coupling from **120** (50 mg, 0.145 mmol, 1.0 equiv). Purification by flash chromatography (hexanes/EtOAc gradient) afforded the methyl ester of the title compound (59 mg, 63%) as a white solid:  $R_f$  = 0.30 (EtOAc);  $^1\text{H}$  NMR (600 MHz,  $\text{CDCl}_3$ )  $\delta$  4.02 (s, 3H), 5.42 (s, 2H), 6.95 (d,  $J$  = 6.0 Hz, 2H), 7.25 (d,  $J$  = 3.0 Hz, 1H), 7.29 (d,  $J$  = 3.0 Hz, 1H), 7.33 (t,  $J$  = 7.2 Hz, 1H), 7.43 (t,  $J$  = 7.2 Hz, 2H), 7.55 (s, 1H), 7.58 (d,  $J$  = 7.2 Hz, 2H), 8.21 (s, 1H), 8.53 (d,  $J$  = 6.0 Hz, 2H);  $^{13}\text{C}$  NMR (150 MHz,  $\text{CDCl}_3$ )  $\delta$  49.3, 52.0, 103.9, 112.5, 121.3, 122.5, 123.4, 127.3, 127.5, 127.7, 129.0, 131.0, 135.4, 137.7, 141.2, 146.3, 150.5, 167.9.

Methyl 6-phenyl-1-(pyridin-4-ylmethyl)-1H-indole-4-carboxylate (50 mg, 0.146 mmol, 1.0 equiv) prepared above was converted to the title compound using the general procedure for ester hydrolysis. Purification by preparative reverse-phase HPLC using method 7 afforded the title compound (9.4 mg, 20%) as a white solid:  $t_R$  = 14.5 min;  $^1\text{H}$  NMR (600 MHz,  $\text{DMSO}-d_6$ )  $\delta$  5.54 (s, 2H), 7.07 (d,  $J$  = 6.0 Hz, 2H), 7.19 (d,  $J$  = 3.0 Hz, 1H), 7.27 (d,  $J$  = 3.0 Hz, 1H), 7.33 (t,  $J$  = 7.2 Hz, 1H), 7.39–7.43 (m, 3H), 7.64 (d,  $J$  = 7.2 Hz, 2H), 7.90 (s, 1H), 8.44 (d,  $J$  = 6.0 Hz, 2H);  $^{13}\text{C}$  NMR (150 MHz,  $\text{DMSO}-d_6$ )  $\delta$  48.1, 104.5, 108.3, 120.7, 121.9, 126.6, 126.9, 128.0, 129.0, 129.6, 133.0, 137.4, 141.9, 148.0, 149.9, 157.0, 170.8; HRMS (ESI–) calcd for  $\text{C}_{21}\text{H}_{15}\text{N}_2\text{O}_2$  [ $\text{M} - \text{H}$ ] $^-$  327.1139, found 327.1145 (error 1.8 ppm).

**Enzyme Binding Studies.** BasE and MbtA were expressed in *E. coli* and purified as described.<sup>38,39</sup> Determination of equilibrium dissociation constants  $K_D$  for each compound was performed using the fluorescence polarization assay with FI-Sal-AMS **14** as ligand in black flat-bottom 96-well plates (Costar no. 3915) as described.<sup>39</sup> A 3-fold serial dilution of each compound (10  $\mu$ L) was added to 90  $\mu$ L of a solution of **14** (20 nM final concentration) and 200 nM BasE or 50 nM MbtA in 30 mM Tris-HCl, pH 7.5, 1 mM  $\text{MgCl}_2$ , and 0.0025% Igepal CA-630. The fluorescence anisotropy was measured after a 30 min incubation at 25  $^\circ\text{C}$ . The  $K_D$  of each compound tested was determined by fitting the displacement curves ( $A_{\text{OBS}}$ , the experimentally measured anisotropy vs  $L_T$ , the test compound concen-



tration) to eqs 1 and 2<sup>46</sup> using Mathematica 7 (Wolfram Research Inc.).

$$A_{\text{OBS}} = \frac{QF_{\text{SB}}A_{\text{B}} + (1 - F_{\text{SB}})A_{\text{F}}}{1 - (1 - Q)F_{\text{SB}}} \quad (1)$$

$$F_{\text{SB}} = \frac{2\sqrt{(a^2 - 3b)} \cos(\theta/3) - a}{3K_{\text{D1}} + 2\sqrt{(a^2 - 3b)} \cos(\theta/3) - a} \quad (2)$$

with

$$a = K_{\text{D1}} + K_{\text{D2}} + L_{\text{ST}} + L_{\text{T}} - R_{\text{T}}$$

$$b = (L_{\text{T}} - R_{\text{T}})K_{\text{D1}} + (L_{\text{ST}} - R_{\text{T}})K_{\text{D2}} + K_{\text{D1}}K_{\text{D2}}$$

$$c = -K_{\text{D1}}K_{\text{D2}}R_{\text{T}}$$

$$\theta = \arccos \left[ \frac{-2a^3 + 9ab - 27c}{2\sqrt{(a^2 - 3b)^3}} \right]$$

In these equations,  $Q$  is the ratio of the fluorescence intensity of the probe in the bound and free states (1.07 for BasE and 1.02 for MbtA<sup>39</sup>),  $F_{\text{SB}}$  is the fraction of bound **14**,  $A_{\text{B}}$  (0.035) and  $A_{\text{F}}$  (0.220 for BasE and 0.308 for MbtA<sup>39</sup>) represent the anisotropies of bound and free probe **14**,  $K_{\text{D1}}$  is the equilibrium dissociation constant of **14** (84.3 nM for BasE and 9.26 nM for MbtA<sup>39</sup>),  $L_{\text{ST}}$  is the concentration of **14**,  $R_{\text{T}}$  is the receptor protein concentration, and  $K_{\text{D2}}$  is the test compound's equilibrium dissociation constant.<sup>46</sup>

**Acinetobacter baumannii MIC Assay.** A single LB agar plate was streaked with 19606 WT and grown overnight at 30 °C. The plate was flooded with 2 mL of medium 1 (M9 minimal medium, 0.2% casamino acids, 200  $\mu\text{M}$  dipyriddy) and transferred to a 15 mL centrifuge tube. Cells were spun down at room temperature and washed twice with 10 mL of medium 1 and then resuspended in 2 mL of medium 1. The  $A_{600}$  was measured, and cells were diluted in medium 1 to an  $A_{600}$  of 1.7–2.0 and then further diluted to 0.0003 in either medium 1 supplemented with 1  $\mu\text{M}$  FeCl<sub>3</sub> or medium 2 (M9 minimal media, 0.2% casamino acids) supplemented with 200  $\mu\text{M}$  FeCl<sub>3</sub>. An amount of 200  $\mu\text{L}$  of each solution was dispensed in triplicate into a 96-well plate containing 2  $\mu\text{L}$  of each inhibitor in DMSO for a final concentration of 100  $\mu\text{M}$ . Tetracycline was used as a positive control (100 ng/mL), and 1% DMSO was used as a negative control. The plates were incubated at 30 °C, and the  $A_{600}$  was measured at 15 h.

**Mycobacterium tuberculosis H37Rv MIC Assay.** Minimum inhibitory concentrations (MICs) were experimentally determined as previously described.<sup>36</sup> MICs were determined in quadruplicate in iron-deficient GAST and GAST supplemented with 200  $\mu\text{M}$  FeCl<sub>3</sub> according to the broth microdilution method using compounds from DMSO stock solutions or with control wells treated with an equivalent amount of DMSO. Isoniazid was used as a positive control, while DMSO was employed as a negative control. All measurements reported herein used an initial cell density of 10<sup>4</sup>–10<sup>5</sup> cells/assay, and growth was monitored at 10–14 days, with the untreated and DMSO-treated control cultures reaching an OD<sub>620</sub> of 0.2–0.3. Plates were incubated at 37 °C (100  $\mu\text{L}$ /well), and growth was recorded by measurement of optical density at 620 nm.

**Protein Crystallography.** The BasE enzyme from *A. baumannii* strain AB900 for crystallographic studies was produced and crystallized as previously described.<sup>31</sup> BasE was cocrystallized with **67** and **70**; crystals were isomorphous with the prior BasE structures. Data were collected at SSRL beamline 11-1. Initial phases were provided by difference Fourier methods using the previous structure of BasE bound to **15** as an initial refinement model; all non-protein atoms were removed prior to refinement. The models were refined to completion as described previously.<sup>31</sup>

**Insertional Deletion of BasE.** Flanking regions of *basE* from *A. baumannii* ATCC 19606 were amplified by PCR using the primers 5'F, 5'R (CACCAGCTCGGATCCACTGGATGTGGTGAGAAGC, CCCGGGACTAGTGACATTCTAAATATTCAATTTAATT-TAATG) and 3'F, 3'R (CACCCGGGCTAGCTAAATAT-

TGAGCAGCATATGG, CCTGCAGGATCCATGTGCTC-TGAAGGACACG). The kanamycin resistance gene (*kanR*) was amplified from pCR2.1 TOPO (Invitrogen) using the primers Kan F, Kan R (CACCAGTGTAAACCGGAATTGCCAGCTGGG, GCTAGCTCAGAAGAACTCGTCAAG). The three PCR fragments were cloned into pENTR/TEV/D-TOPO (Invitrogen) for ease of propagation creating pCDD129, pCDD130, and pCDD131 for the 5', KanR, and 3' fragments respectively. The knockout fragments were cloned sequentially into pUC18 by first ligating the 5' fragment after digesting pCDD129 and pUC18 with *SacI* and *SmaI*, creating pCDD132. The 3' fragment was added next by ligating *SmaI*, *SbfI* digested pCDD131, and pCDD132, creating pCDD133. KanR was removed from pCDD130 by digestion with *SpeI*, *NheI* and ligated into similarly cut pCDD133, creating pCDD134. The knockout cassette was removed from pCDD134 by digestion with *BamHI* and cloned into pKC1139, a *Streptomyces/E. coli* shuttle vector to create pCDD135, which will act as a suicide vector in *A. baumannii*. The knockout plasmid was transformed into ATCC 19606 using electroporation as previously described.<sup>64,65</sup> Clones resistant to kanamycin and sensitive to apramycin were confirmed by PCR to have the correct genome insertion using the primer pairs 5' confirm (CACCACGAGGTATTTTGTGCTGGG), KanR, and KanF, 3' confirm (CACCACGAGGTATTTTGTGCTGGG), creating 19606  $\Delta\text{basE}$ .

**Complementation of 19606  $\Delta\text{basE}$ .** The *E. coli*, *A. baumannii* shuttle vector pWH1266 (ATCC, Manassas, VA) was used to complement 19606  $\Delta\text{basE}$ . The primers *basE* comp F (CACCAGTCTTGTGAATCATTTCCAATTTTG) and *basE* comp R (GCATGCTTAAGATGTTGTAGATGTATTTAAATGC) were used to PCR amplify *basE* and its promoter region from ATCC19606. Primers Apr F (CACCAAGCTTTAAGGTTTCATGTGCAGCTCCATC) and Apr R (GGATCCTCAGCCAATCGACTGGCG) were used to amplify the apramycin resistance (*aprR*) gene from pKC1139. The *basE* fragment was digested with *BamHI* and *SphI*, and AprR was digested with *BamHI* and *HindIII*. Both fragments were ligated into pWH1266 digested with *HindIII* and *SphI*, creating pCDD140. The final plasmid was transformed into 19606  $\Delta\text{basE}$  using the method described above.

**Growth of *A. baumannii* Strains.** LB agar plates were streaked with 19606 WT, 19606  $\Delta\text{basE}$ , or 19606  $\Delta\text{basE}$  pCDD140 and grown overnight at 30 °C. Each plate was flooded with 2 mL of medium 1 (M9 minimal medium, 0.2% casamino acids, 200  $\mu\text{M}$  dipyriddy) and transferred to a 15 mL centrifuge tube. Cells were spun down at room temperature and washed twice with 10 mL of medium 1 and then resuspended in 2 mL of medium 1. The  $A_{600}$  was measured, and cells were diluted in medium 1 to an  $A_{600}$  of 1.7–2.0 and then further diluted to 0.0003 in either medium 1 supplemented with 1  $\mu\text{M}$  FeCl<sub>3</sub> or medium 2 (M9 minimal medium, 0.2% casamino acids) supplemented with 200  $\mu\text{M}$  FeCl<sub>3</sub> and placed into a 96-well plate in six 200  $\mu\text{L}$  replicates. Positive controls for iron limiting and rich conditions consisted of WT supplemented with 100 ng/mL tetracycline. The plates were incubated at 30 °C, and the  $A_{600}$  was measured at 2, 4, 6, 7, 8, 9, 10, 12, 13, and 22 h.

## ■ ASSOCIATED CONTENT

### ■ Supporting Information

Synthetic procedures and characterization data for compounds **23–25**, **27**, **28**, **37–62**, and **64–92** and representative <sup>1</sup>H and <sup>13</sup>C NMR spectra for **15–19**, **21**, **22**, **37**, **60**, **63**, **91**, **94**, and **98**. This material is available free of charge via the Internet at <http://pubs.acs.org>.

## ■ AUTHOR INFORMATION

### Corresponding Author

\*Phone: 612-625-7956. Fax: 612-626-5173. E-mail: [aldri015@umn.edu](mailto:aldri015@umn.edu).

## Present Address

<sup>†</sup>For J.N.: Global Health Institute, École Polytechnique Fédérale de Lausanne, 1015 Lausanne, Switzerland. E-mail: joao.neres@epfl.ch.

## Notes

The authors declare no competing financial interest.

## ■ ACKNOWLEDGMENTS

This research was supported by grants from the National Institutes of Health (Grant AI070219 to C.C.A. and Grant GM-068440 to A.M.G.) and the Intramural Research Program of the NIAID in the National Institutes of Health (to C.E.B.). We thank Dr. Michael Walters (Institute for Therapeutics Discovery and Development, University of Minnesota) for assistance with the parallel synthesis and Prof. David H. Sherman (Life Sciences Institute, University of Michigan) for plasmids pUC18 and pKC1139.

## ■ ABBREVIATIONS USED

AAAE, aryl acid adenylating enzyme; ArCP, aryl carrier protein; BOP, (benzotriazol-1-yloxy)tris(dimethylamino)phosphonium hexafluorophosphate; DHB, 2,3-dihydroxybenzoic acid; DHB-AMS, 5'-O-[N-(2,3-dihydroxybenzoyl)sulfamoyl]adenosine; Fl-Sal-AMS, 2'-O-{2-[2-(2-[(fluorescein-5-yl)carbonyl]amino)-ethoxy]ethoxy}ethoxy-5'-O-[N-(salicyl)sulfamoyl]adenosine; FP, fluorescence polarization; HPLC, high-performance liquid chromatography; HTS, high-throughput screening; MDR, multidrug resistant; MIC, minimum inhibitory concentration; NRPS, nonribosomal peptide synthetase; PMP, *p*-methoxyphenyl; PyBroP, bromotripyrrolidinophosphonium hexafluorophosphate; ROS, reactive oxygen species; SAL, salicylic acid; Sal-AMS, 5'-O-[N-(salicyl)sulfamoyl]adenosine; SAR, structure-activity relationship; TES, triethylsilyl; TFA, trifluoroacetic acid

## ■ REFERENCES

- (1) Projan, S. J.; Bradford, P. A. Late stage antibacterial drugs in the clinical pipeline. *Curr. Opin. Microbiol.* **2007**, *10*, 441–446.
- (2) Wright, G. D. Antibiotics: a new hope. *Chem. Biol.* **2012**, *19*, 3–10.
- (3) Peleg, A. Y.; Seifert, H.; Paterson, D. L. *Acinetobacter baumannii*: emergence of a successful pathogen. *Clin. Microbiol. Rev.* **2008**, *21*, 538–582.
- (4) Calhoun, J. H.; Murray, C. K.; Manring, M. M. Multidrug-resistant organisms in military wounds from Iraq and Afghanistan. *Clin. Orthop. Relat. Res.* **2008**, *466*, 1356–1362.
- (5) Lockhart, S. R.; Abramson, M. A.; Beekmann, S. E.; Gallagher, G.; Riedel, S.; Diekema, D. J.; Quinn, J. P.; Doern, G. V. Antimicrobial resistance among Gram-negative bacilli causing infections in intensive care unit patients in the United States between 1993 and 2004. *J. Clin. Microbiol.* **2007**, *45*, 3352–3359.
- (6) Rhomberg, P. R.; Jones, R. N. Summary trends for the Meropenem Yearly Susceptibility Test Information Collection Program: a 10-year experience in the United States (1999–2008). *Diagn. Microbiol. Infect. Dis.* **2009**, *65*, 414–426.
- (7) Vallenet, D.; Nordmann, P.; Barbe, V.; Poirel, L.; Mangenot, S.; Bataille, E.; Dossat, C.; Gas, S.; Kreimeyer, A.; Lenoble, P.; Oztas, S.; Poulain, J.; Segurens, B.; Robert, C.; Abergel, C.; Claverie, J. M.; Raoult, D.; Medigue, C.; Weissenbach, J.; Cruveiller, S. Comparative analysis of *Acinetobacter*: three genomes for three lifestyles. *PLoS One* **2008**, *3*, e1805.
- (8) Adams, M. D.; Goglin, K.; Molyneaux, N.; Hujer, K. M.; Lavender, H.; Jamison, J. J.; MacDonald, I. J.; Martin, K. M.; Russo, T.; Campagnari, A. A.; Hujer, A. M.; Bonomo, R. A.; Gill, S. R.

Comparative genome sequence analysis of multidrug-resistant *Acinetobacter baumannii*. *J. Bacteriol.* **2008**, *190*, 8053–8064.

- (9) Falagas, M. E.; Kasiakou, S. K. Colistin: the revival of polymyxins for the management of multidrug-resistant Gram-negative bacterial infections. *Clin. Infect. Dis.* **2005**, *40*, 1333–1341.

- (10) Cai, Y.; Chai, D.; Wang, R.; Liang, B.; Bai, N. Colistin resistance of *Acinetobacter baumannii*: clinical reports, mechanisms and antimicrobial strategies. *J. Antimicrob. Chemother.* **2012**, *67*, 1607–1615.

- (11) Posey, J. E.; Gherardini, F. C. Lack of a role for iron in the lyme disease pathogen. *Science* **2000**, *288*, 1651–1653.

- (12) Miethke, M.; Marahiel, M. A. Siderophore-based iron acquisition and pathogen control. *Microbiol. Mol. Biol. Rev.* **2007**, *71*, 413–451.

- (13) Crosa, J. H.; Walsh, C. T. Genetics and assembly line enzymology of siderophore biosynthesis in bacteria. *Microbiol. Mol. Biol. Rev.* **2002**, *66*, 223–249.

- (14) Sandy, M.; Butler, A. Microbial iron acquisition: marine and terrestrial siderophores. *Chem. Rev.* **2009**, *109*, 4580–4595.

- (15) Hider, R. C.; Kong, X. Chemistry and biology of siderophores. *Nat. Prod. Rep.* **2010**, *27*, 637–657.

- (16) Zimblar, D. L.; Penwell, W. F.; Gaddy, J. A.; Menke, S. M.; Tomaras, A. P.; Connerly, P. L.; Actis, L. A. Iron acquisition functions expressed by the human pathogen *Acinetobacter baumannii*. *BioMetals* **2009**, *22*, 23–32.

- (17) Lawlor, M. S.; O'Connor, C.; Miller, V. L. Yersiniabactin is a virulence factor for *Klebsiella pneumoniae* during pulmonary infection. *Infect. Immun.* **2007**, *75*, 1463–1472.

- (18) Takase, H.; Nitani, H.; Hoshino, K.; Otani, T. Impact of siderophore production on *Pseudomonas aeruginosa* infections in immunosuppressed mice. *Infect. Immun.* **2000**, *68*, 1834–1839.

- (19) Fischbach, M. A.; Lin, H.; Zhou, L.; Yu, Y.; Abergel, R. J.; Liu, D. R.; Raymond, K. N.; Wanner, B. L.; Strong, R. K.; Walsh, C. T.; Aderem, A.; Smith, K. D. The pathogen-associated *iroA* gene cluster mediates bacterial evasion of lipocalin 2. *Proc. Natl. Acad. Sci. U.S.A.* **2006**, *103*, 16502–16507.

- (20) Cendrowski, S.; MacArthur, W.; Hanna, P. *Bacillus anthracis* requires siderophore biosynthesis for growth in macrophages and mouse virulence. *Mol. Microbiol.* **2004**, *51*, 407–417.

- (21) Dale, S. E.; Doherty-Kirby, A.; Lajoie, G.; Heinrichs, D. E. Role of siderophore biosynthesis in virulence of *Staphylococcus aureus*: identification and characterization of genes involved in production of a siderophore. *Infect. Immun.* **2004**, *72*, 29–37.

- (22) De Voss, J. J.; Rutter, K.; Schroeder, B. G.; Su, H.; Zhu, Y.; Barry, C. E., 3rd. The salicylate-derived mycobactin siderophores of *Mycobacterium tuberculosis* are essential for growth in macrophages. *Proc. Natl. Acad. Sci. U.S.A.* **2000**, *97*, 1252–1257.

- (23) Kohanski, M. A.; Dwyer, D. J.; Hayete, B.; Lawrence, C. A.; Collins, J. J. A common mechanism of cellular death induced by bactericidal antibiotics. *Cell* **2007**, *130*, 797–810.

- (24) Dwyer, D. J.; Kohanski, M. A.; Collins, J. J. Role of reactive oxygen species in antibiotic action and resistance. *Curr. Opin. Microbiol.* **2009**, *12*, 482–489.

- (25) Yamamoto, S.; Okujo, N.; Sakakibara, Y. Isolation and structure elucidation of acinetobactin, a novel siderophore from *Acinetobacter baumannii*. *Arch. Microbiol.* **1994**, *162*, 249–254.

- (26) Takeuchi, Y.; Ozaki, S.; Satoh, M.; Mimura, K.; Hara, S.; Abe, H.; Nishioka, H.; Harayama, T. Synthesis of acinetobactin. *Chem. Pharm. Bull.* **2010**, *58*, 1552–1553.

- (27) Dorsey, C. W.; Tomaras, A. P.; Connerly, P. L.; Tolmasky, M. E.; Crosa, J. H.; Actis, L. A. The siderophore-mediated iron acquisition systems of *Acinetobacter baumannii* ATCC 19606 and *Vibrio anguillarum* 775 are structurally and functionally related. *Microbiology* **2004**, *150*, 3657–3667.

- (28) Mihara, K.; Tanabe, T.; Yamakawa, Y.; Funahashi, T.; Nakao, H.; Narimatsu, S.; Yamamoto, S. Identification and transcriptional organization of a gene cluster involved in biosynthesis and transport of acinetobactin, a siderophore produced by *Acinetobacter baumannii* ATCC 19606T. *Microbiology* **2004**, *150*, 2587–2597.



- (29) Sattely, E. S.; Walsh, C. T. A latent oxazoline electrophile for N-O-C bond formation in pseudomonine biosynthesis. *J. Am. Chem. Soc.* **2008**, *130*, 12282–12284.
- (30) Wuest, W. M.; Sattely, E. S.; Walsh, C. T. Three siderophores from one bacterial enzymatic assembly line. *J. Am. Chem. Soc.* **2009**, *131*, 5056–5057.
- (31) Drake, E. J.; Duckworth, B. P.; Neres, J.; Aldrich, C. C.; Gulick, A. M. Biochemical and structural characterization of bisubstrate inhibitors of BasE, the self-standing nonribosomal peptide synthetase adenylate-forming enzyme of acinetobactin synthesis. *Biochemistry* **2010**, *49*, 9292–9305.
- (32) Hurdle, J. G.; O'Neill, A. J.; Chopra, I. Prospects for aminoacyl-tRNA synthetase inhibitors as new antimicrobial agents. *Antimicrob. Agents Chemother.* **2005**, *49*, 4821–4833.
- (33) Sikora, A. L.; Wilson, D. J.; Aldrich, C. C.; Blanchard, J. S. Kinetic and inhibition studies of dihydroxybenzoate-AMP ligase from *Escherichia coli*. *Biochemistry* **2010**, *49*, 3648–3657.
- (34) Gulick, A. M. Conformational dynamics in the Acyl-CoA synthetases, adenylation domains of non-ribosomal peptide synthetases, and firefly luciferase. *ACS Chem. Biol.* **2009**, *4*, 811–827.
- (35) Ferreras, J. A.; Ryu, J. S.; Di Lello, F.; Tan, D. S.; Quadri, L. E. Small-molecule inhibition of siderophore biosynthesis in *Mycobacterium tuberculosis* and *Yersinia pestis*. *Nat. Chem. Biol.* **2005**, *1*, 29–32.
- (36) Somu, R. V.; Boshoff, H.; Qiao, C. H.; Bennett, E. M.; Barry, C. E.; Aldrich, C. C. Rationally designed nucleoside antibiotics that inhibit siderophore biosynthesis of *Mycobacterium tuberculosis*. *J. Med. Chem.* **2006**, *49*, 31–34.
- (37) Miethke, M.; Bissleret, P.; Beckering, C. L.; Vignard, D.; Eustache, J.; Marahiel, M. A. Inhibition of aryl acid adenylation domains involved in bacterial siderophore synthesis. *FEBS J.* **2006**, *273*, 409–419.
- (38) Somu, R. V.; Wilson, D. J.; Bennett, E. M.; Boshoff, H. I.; Celia, L.; Beck, B. J.; Barry, C. E.; Aldrich, C. C. Antitubercular nucleosides that inhibit siderophore biosynthesis: SAR of the glycosyl domain. *J. Med. Chem.* **2006**, *49*, 7623–7635.
- (39) Neres, J.; Wilson, D. J.; Celia, L.; Beck, B. J.; Aldrich, C. C. Aryl acid adenylating enzymes involved in siderophore biosynthesis: fluorescence polarization assay, ligand specificity, and discovery of non-nucleoside inhibitors via high-throughput screening. *Biochemistry* **2008**, *47*, 11735–11749.
- (40) Hohn, H. Ein neue Verfahren zur Darstellung von 5-Aminopyrazolen. *Z. Chem.* **1970**, *10*, 386–388.
- (41) Dorn, H.; Müller, T. Zur direkten (C-4)-substitution von Amino-Pyrazolen mit  $\beta$ -keto-carbonyl-Verbindungen—1-Benzyl-6, 7-dihydro-4-ethoxycarbonyl-6-oxo-pyrazolo[3,4-*b*]pyridin. *Z. Chem.* **1980**, *20*, 95.
- (42) Kang, F. A.; Sui, Z. H.; Murray, W. V. Pd-catalyzed direct arylation of tautomerizable heterocycles with aryl boronic acids via C-OH bond activation using phosphonium salts. *J. Am. Chem. Soc.* **2008**, *130*, 11300–11302.
- (43) Wan, Z. K.; Wacharasindhu, S.; Levins, C. G.; Lin, M.; Tabei, K.; Mansour, T. S. The scope and mechanism of phosphonium-mediated S(N)Ar reactions in heterocyclic amides and ureas. *J. Org. Chem.* **2007**, *72*, 10194–10210.
- (44) Gupte, A.; Boshoff, H. I.; Wilson, D. J.; Neres, J.; Labello, N. P.; Somu, R. V.; Xing, C.; Barry, C. E.; Aldrich, C. C. Inhibition of siderophore biosynthesis by 2-triazole substituted analogues of 5'-O-[N-(salicyl)sulfamoyl]adenosine: antibacterial nucleosides effective against *Mycobacterium tuberculosis*. *J. Med. Chem.* **2008**, *51*, 7495–7507.
- (45) Shi, C.; Aldrich, C. C. Efficient Pd-catalyzed coupling of tautomerizable heterocycles with terminal alkynes via C-OH bond activation using PyBroP. *Org. Lett.* **2010**, *12*, 2286–2289.
- (46) Roehrl, M. H. A.; Wang, J. Y.; Wagner, G. A general framework for development and data analysis of competitive high-throughput screens for small-molecule inhibitors of protein–protein interactions by fluorescence polarization. *Biochemistry* **2004**, *43*, 16056–16066.
- (47) Stachelhaus, T.; Mootz, H. D.; Marahiel, M. A. The specificity-conferring code of adenylation domains in nonribosomal peptide synthetases. *Chem. Biol.* **1999**, *6*, 493–505.
- (48) Auld, D. S.; Lovell, S.; Thorne, N.; Lea, W. A.; Maloney, D. J.; Shen, M.; Rai, G.; Battaile, K. P.; Thomas, C. J.; Simeonov, A.; Hanzlik, R. P.; Inglese, J. Molecular basis for the high-affinity binding and stabilization of firefly luciferase by PTC124. *Proc. Natl. Acad. Sci. U.S.A.* **2010**, *107*, 4878–4883.
- (49) Lee, T. V.; Johnson, L. J.; Johnson, R. D.; Koulman, A.; Lane, G. A.; Lott, J. S.; Arcus, V. L. Structure of a eukaryotic nonribosomal peptide synthetase adenylation domain that activates a large hydroxamate amino acid in siderophore biosynthesis. *J. Biol. Chem.* **2010**, *285*, 2415–2427.
- (50) Gordon, N. C.; Wareham, D. W. Multidrug-resistant *Acinetobacter baumannii*: mechanisms of virulence and resistance. *Int. J. Antimicrob. Agents* **2010**, *35*, 219–226.
- (51) Quadri, L. E. Strategic paradigm shifts in the antimicrobial drug discovery process of the 21st century. *Infect. Disord. Drug Targets* **2007**, *7*, 230–237.
- (52) Frederick, R. E.; Mayfield, J. A.; DuBois, J. L. Iron trafficking as an antimicrobial target. *BioMetals* **2009**, *22*, 583–593.
- (53) Ballouche, M.; Cornelis, P.; Baysse, C. Iron metabolism: a promising target for antibacterial strategies. *Recent Pat. Anti-Infect. Drug Discovery* **2009**, *4*, 190–205.
- (54) Cescau, S.; Cwerman, H.; Letoffe, S.; Delepelaire, P.; Wandersman, C.; Biville, F. Heme acquisition by hemophores. *BioMetals* **2007**, *20*, 603–613.
- (55) Budzikiewicz, H. *Microbial Siderophores*; Springer-Verlag: Vienna, Austria, 2010; Vol. 92, p 75.
- (56) Fischbach, M. A.; Walsh, C. T. Antibiotics for emerging pathogens. *Science* **2009**, *325*, 1089–1093.
- (57) Adler, C.; Corbalan, N. S.; Seyedsayam, M. R.; Pomares, M. F.; de Cristobal, R. E.; Clardy, J.; Kolter, R.; Vincent, P. A. Catecholate siderophores protect bacteria from pyochelin toxicity. *PLoS One* **2012**, *7*, e46754.
- (58) Dorsey, C. W.; Tolmasky, M. E.; Crosa, J. H.; Actis, L. A. Genetic organization of an *Acinetobacter baumannii* chromosomal region harbouring genes related to siderophore biosynthesis and transport. *Microbiology* **2003**, *149*, 1227–1238.
- (59) Penwell, W. F.; Arivett, B. A.; Actis, L. A. The *Acinetobacter baumannii* entA gene located outside the acinetobactin cluster is critical for siderophore production, iron acquisition and virulence. *PLoS One* **2012**, *7*, e36493.
- (60) Gaddy, J. A.; Arivett, B. A.; McConnell, M. J.; Lopez-Rojas, R.; Pachon, J.; Actis, L. A. Role of acinetobactin-mediated iron acquisition functions in the interaction of *Acinetobacter baumannii* strain ATCC 19606T with human lung epithelial cells, *Galleria mellonella* caterpillars, and mice. *Infect. Immun.* **2012**, *80*, 1015–1024.
- (61) Eijkelkamp, B. A.; Hassan, K. A.; Paulsen, I. T.; Brown, M. H. Investigation of the human pathogen *Acinetobacter baumannii* under iron limiting conditions. *BMC Genomics* **2011**, *12*, 126.
- (62) Antunes, L. C.; Imperi, F.; Towner, K. J.; Visca, P. Genome-assisted identification of putative iron-utilization genes in *Acinetobacter baumannii* and their distribution among a genotypically diverse collection of clinical isolates. *Res. Microbiol.* **2011**, *162*, 279–284.
- (63) Misra, R. N.; Rawlins, D. B.; Xiao, H. Y.; Shan, W. F.; Bursuker, I.; Kellar, K. A.; Mulheron, J. G.; Sack, J. S.; Tokarski, J. S.; Kimball, S. D.; Webster, K. R. 1H-Pyrazolo[3,4-*b*]pyridine inhibitors of cyclin-dependent kinases. *Bioorg. Med. Chem. Lett.* **2003**, *13*, 1133–1136.
- (64) Higgins, P. G.; Poirel, L.; Lehmann, M.; Nordmann, P.; Seifert, H. OXA-143, a novel carbapenem-hydrolyzing class D beta-lactamase in *Acinetobacter baumannii*. *Antimicrob. Agents Chemother.* **2009**, *53*, 5035–5038.
- (65) Choi, K. H.; Kumar, A.; Schweizer, H. P. A 10-min method for preparation of highly electrocompetent *Pseudomonas aeruginosa* cells: application for DNA fragment transfer between chromosomes and plasmid transformation. *J. Microbiol. Methods* **2006**, *64*, 391–397.